Field-field and photon-photon interferometry

Optical interferometry was at the heart of the revolution which ushered in the new era of twentieth century physics. For example, the Michelson interferometer was used to show that there is no detectable motion relative to the 'ether'; a key experiment in support of special relativity.

It is a wonderful tribute to Michelson that the same interferometer concept is central to the gravity-wave detectors which promise to provide new insights into general relativity and astrophysics in the twenty-first century. Similar tales can be told about the Sagnac and Mach-Zehnder interferometers as discussed in this chapter. We further note that the intensity correlation stellar interferometer of Hanbury-Brown and Twiss* was a driving force in ushering in the modern era of quantum optics.

We are thus motivated to develop the theory of field (amplitude) and photon (intensity) correlation interferometry. In doing so we will find that the subject provides us with an exquisite probe of the micro and macrocosmos, i.e., quantum mechanics and general relativity.

With these thoughts in mind we here develop a framework to study the quantum statistical correlations of light. We will motivate the quantum correlation functions of the field operators from the standpoint of photodetection theory. Many experimentally observed quantities, such as photoelectron statistics and the spectral distribution of the field, can be related to the appropriate field correlation functions. These correlation functions are essential in the description of Young's double-slit experiment and the notion of the power spectrum of light. The intensity correlation functions are usually associated with the intensity—intensity correlation measurements as required in

^{*} See the pioneering work of Hanbury-Brown and Twiss [1954, 1956]. Excellent pedagogical treatments of the problem are given by Fano [1961], Glauber [1965], and Baym [1969]. For a review of the subject see Hanbury-Brown [1974].

the descriptions of the famous Hanbury-Brown-Twiss effect and other two-photon interference experiments which we discuss in this chapter.

Quantum coherence theory also allows us to examine field states which exhibit certain nonclassical features, i.e., states which cannot be described by a classical statistical theory. Such states can arise when the quantum nature of light is explicitly exhibited. Examples are the number and squeezed states of the radiation field.

In the next two sections we discuss the application of interferometry to astrophysics and general relativity and then turn to a general discussion of photon optics.

4.1 The interferometer as a cosmic probe

The foundations of physics are anchored in the bedrock of curved spacetime. 'Spacetime' in the sense of Minkowski who showed us that physical events (e.g., the emission of a photon) are best viewed as occurring in a (flat) four-dimensional geometry having one time and three spatial coordinates. The adjective 'curved' enters the picture when gravitation is included in the problem. That is, according to Einstein's theory of general relativity, we view gravity as arising from (or described by) the curvature of this four-dimensional space. This curvature itself is produced by the presence of massive bodies in the universe, the earth, sun, Crab Nebula, etc.

Many theorists regard the general theory of relativity to be the most beautiful of all physical theories. However, due to the smallness of the gravitational coupling constant,

$$G = 6.67 \times 10^{-8} \text{ cm}^3/\text{g s}^2$$
,

experimental tests of this theory are very scarce. This fact is underscored by Misner, Thorne, and Wheeler, who observed that: 'For the first half century of its life, general relativity was a theorist's paradise but an experimentalist's hell.' However, thanks in large part to advances in modern laser optics, new tests of metric gravity (general relativity) have been, and will continue to be, carried out. The optical interferometer is the main tool in these astrophysical and general relativistic studies.

4.1.1 Michelson interferometer and general relativity

As mentioned earlier, the Michelson interferometer was used to search for motion through the ether and was one of the key experiments in formulating special relativity and modern physics.

At present a type of Michelson interferometer is being built to detect gravity waves. As depicted in Fig. 4.1, gravitational radiation acts so as to effectively change the path length for light in one arm of the interferometer and thus introduces a phase shift. How this phase shift comes about can be viewed in two different ways: (1) the gravity wave changes the distance between the mirrors (2) the gravity wave changes or perturbes spacetime and acts much as a dielectric. We here take the first point of view.

In time-independent (Newtonian) gravity, the (scalar) potential Φ (in free space) obeys the Laplace equation

$$\nabla^2 \Phi = 0, \tag{4.1.1}$$

whereas, in time-dependent (Einsteinian) metric gravity, the tensor field* $\Phi_{\mu\nu}(\mathbf{r},t)$, where the indices μ and ν run from 1 to 4, obeys a wave equation of the form

$$\left(\nabla^2 - \frac{1}{c^2} \frac{\partial^2}{\partial t^2}\right) \Phi_{\mu\nu}(\mathbf{r}, t) = 0. \tag{4.1.2}$$

Thus, the effects of gravity propagate with the speed of light c from their point of origin (binary stars, exploding galaxies, etc.) to our laboratory on earth. This 'gravitational wave' causes points in the laboratory to experience tiny amplitude-relative oscillations.

A scheme to measure the gravitational waves (g-waves) is based on the Michelson interferometer. The effect of gravitational radiation is to stretch or compress a rod of length L which is perpendicular to the direction of propagation. For example, the gravitational wave of frequency v_g will cause the length L_x between the mirror M_1 and the beam-splitter in Fig. 4.1(a) to vary as

$$L_x = L[1 + h_0 \cos(v_g t)], \tag{4.1.3}$$

where L is the length of the interferometer arm in the absence of a gravitational wave and h_0 represents the amplitude of the gravitational wave and is of order $\leq 10^{-21}$ for the envisioned sources.

Therefore, there will be a phase shift between the light traversing the two arms of the interferometer of an amount

$$\delta = k(L_x - L_y)$$

$$= kLh_0 \cos(v_g t). \tag{4.1.4}$$

Hence the intensity recorded by the detector in Fig. 4.1(a) will be

For a discussion of general relativity directed toward the student of modern quantum optics see Schleich and Scully [1984].

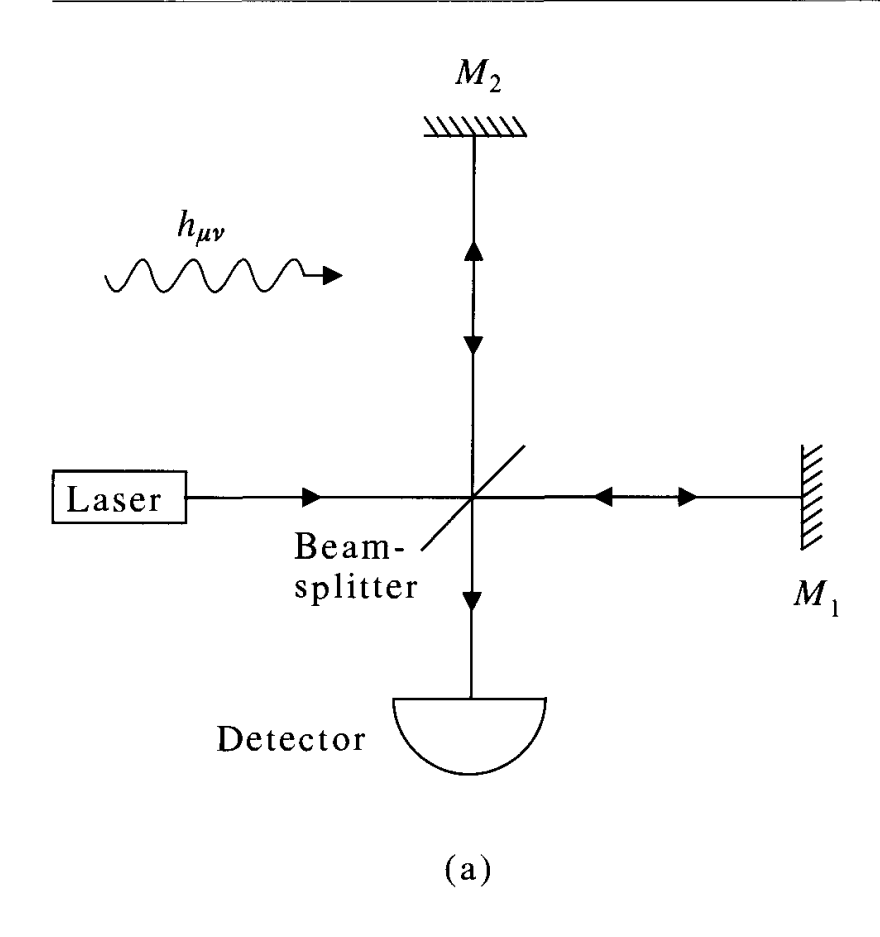
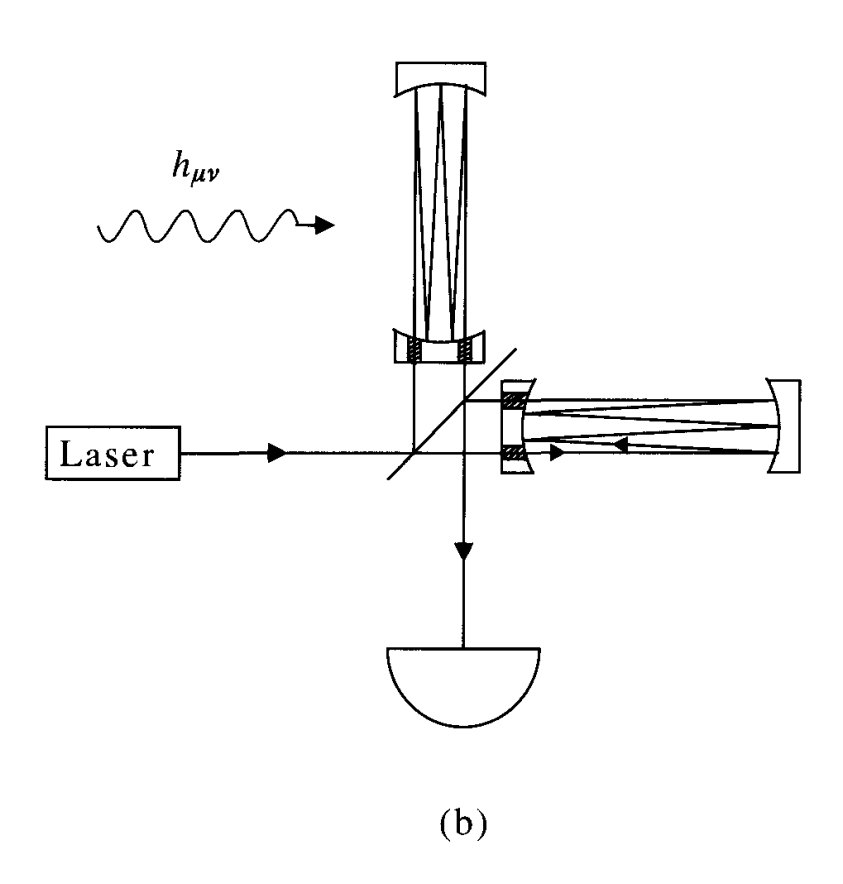


Fig. 4.1
(a) An external laser drives a Michelson interferometer which is indluenced by an incident gravity wave denoted by $h_{\mu\nu}$. (b) A Michelson interferometer with cavities in both arms. 'folds' the light many times, thus lengthening the effective optical path lengths in each arm.



$$I = \frac{1}{2}I_0(1 + \cos \delta),\tag{4.1.5}$$

where I_0 is the incident intensity.

In the actual experiments, cavities are used in the two arms of the Michelson interferometer as in Fig. 4.1(b). Now the signal due to a gravity wave translates into a time-dependent phase shift obtained from Eq. (4.1.4) by replacing L_x by the effective path length \tilde{L} , which is essentially the number of bounces times the length of the arm L. Therefore, for times $t \ll v_g^{-1}$, the g-wave-induced phase shift is given by $\Delta \theta^{(p)} = v \tilde{L} h_0/c$, where v is the frequency of the laser light. In such an experiment the fundamental quantum limit is given by 'photon shot noise'. Denoting the average number of laser photons by \bar{n} , the power at the detector by P and assuming unit quantum efficiency for present purposes, one has the phase uncertainty due to shot noise for a measurement of duration t_m

$$\Delta\theta_n \simeq \frac{1}{\sqrt{\bar{n}}} = \sqrt{\frac{\hbar v}{P t_m}}.$$
 (4.1.6)

Equating $\Delta\theta^{(p)}$ to $\Delta\theta_n$, we find the minimum detectable g-wave amplitude for such a passive system to be

$$h_{\min}^{(p)} \simeq \frac{c}{v\tilde{L}} \sqrt{\frac{\hbar v}{P t_m}} = \frac{\mathscr{C}}{v} \sqrt{\frac{\hbar v}{P t_m}},$$
 (4.1.7)

where we have introduced the cavity decay rate $\mathscr{C} = c/\tilde{L}$.

4.1.2 The Sagnac ring interferometer

In 1913 Sagnac considered the use of a ring resonator to search for the 'ether drift' relative to a rotating frame. However, as often happens, his results turned out to be useful in ways that Sagnac himself never dreamt of. As shown in Fig. 4.2, the real physics associated with the Sagnac effect is simply that it takes longer for a short pulse of light to 'get back' to its point of origin if it goes in the direction of rotation and it takes less time if it is moving in a counter-propagating sense.

To quantify this, consider Fig. 4.2. There we see that laser light enters the interferometer at point A and is split into clockwise (CW) and counter-clockwise (CCW) propagating beams by a beam-splitter. If the interferometer is not rotating, the CW and CCW propagating beams recombine at point A after a time given by

$$t = \frac{2\pi b}{c},\tag{4.1.8}$$

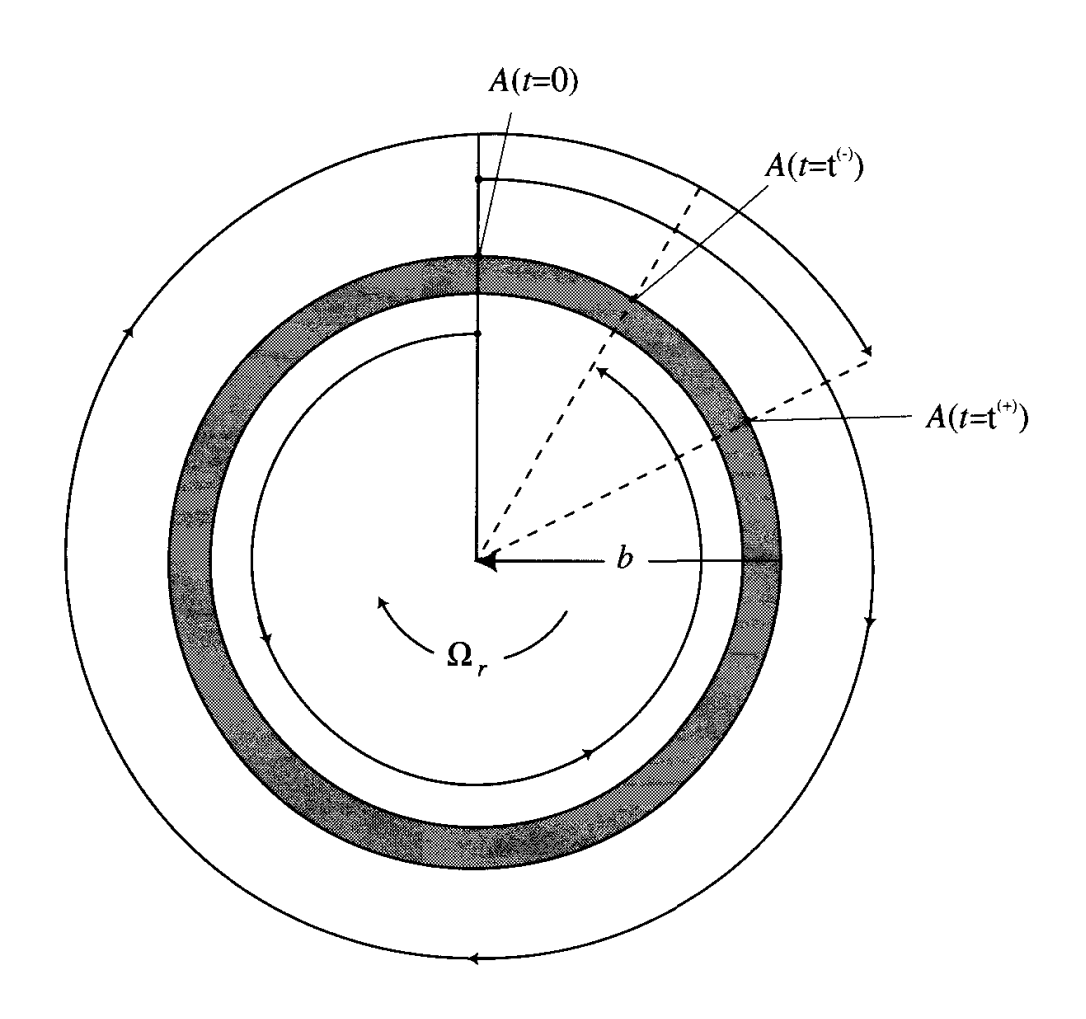


Fig. 4.2 Schematics of a Sagnac ring interferometer.

where b is the radius of the circular beam path. However, if the interferometer is rotating, with angular velocity Ω_r , about an axis through the center and perpendicular to the plane of the interferometer, then the beams reencounter the beam-splitter at different times because the CW (co-directional with Ω_r) propagating beam must traverse a path length of slightly more than $2\pi b$ in order to complete one round trip, since the interferometer rotates through a small angle during the round-trip transit time. Similarly, the CCW propagating beam traverses a path length slightly less than $2\pi b$ during one round trip. If we denote the round-trip transit time of the CW beam by t^+ and that of the CCW beam by t^- , then t^+ is given by

$$t^{+} = \frac{2\pi b + b\Omega_{r}t^{+}}{c}$$

$$= \frac{2\pi b}{c} \left(1 - \frac{b\Omega_{r}}{c}\right)^{-1}, \qquad (4.1.9a)$$

where, in the first line, $b\Omega_r t^+$ is the arc length the interferometer rotates through before the CW beam arrives back at the beam-splitter.

Similarly,

$$t^{-} = \frac{2\pi b - b\Omega_r t^{-}}{c}$$

$$= \frac{2\pi b}{c} \left(1 + \frac{b\Omega_r}{c} \right)^{-1}.$$
(4.1.9b)

The difference between t^+ and t^- is given by

$$\Delta t = t^{+} - t^{-} = \frac{4\pi b^{2} \Omega_{r}}{c^{2} - b^{2} \Omega_{r}^{2}}.$$
(4.1.10)

For reasonable values of b and Ω_r , $(b\Omega_r)^2 \ll c^2$, so that

$$\Delta t \cong \frac{4\pi b^2 \Omega_r}{c^2},\tag{4.1.11}$$

the round-trip optical path difference, ΔL , is given by

$$\Delta L = c\Delta t = \frac{4\pi b^2 \Omega_r}{c}. (4.1.12)$$

From Eq. (4.1.12) we see the round-trip optical path difference, according to this analysis, is directly proportional to the rotation rate of the interferometer. A more general approach valid for an arbitrary interferometer shape leads to the result

$$\Delta L = \frac{4\Omega_r \cdot \hat{\mathbf{z}}A}{C},\tag{4.1.13}$$

where A is the area enclosed by the light path and \hat{z} is a unit vector normal to the surface of the interferometer.

The effectiveness of the Sagnac interferometer is limited by the fact that the optical path difference given by Eq. (4.1.12) is much less than a wavelength. (For instance, if b=1 m and $\Omega_r=10$ deg/h, then $\Delta L\cong 4.1\times 10^{-12}$ m.) At first glance this would seem to make the use of ring laser gyros impractical as rotation sensing devices, since sensitivities of 10^{-3} deg/h or less are desirable. However, there are two different schemes used to greatly increase the sensitivity of ring laser gyros.

The first of these is to increase the total round-trip path length of the light by the use of a kilometer-long optical fiber as the interferometer cavity. To see why this increases the sensitivity of the gyroscope, we shall recast Eq. (4.1.12) into a more general form. From Eq. (4.1.12) we see that the phase difference, $\Delta\theta$, between the counter-propagating beams after one round trip is given by

$$\Delta\theta = \frac{2\pi\Delta L}{\lambda} = \frac{8\pi^2 b^2 \Omega_r}{c\lambda} = \frac{4A\Omega_r}{c\bar{\lambda}},\tag{4.1.14}$$

where $\bar{\lambda} = \lambda/2\pi$ is the reduced wavelength of the laser light and $A = \pi b^2$ is the area enclosed by the light beams. Equation (4.1.14) is valid for a one loop circular light path. If an optical fiber is used, the light path typically consists of a fiber coil of radius b and many turns. In particular, in such a fiber coil with N turns, Eq. (4.1.14) becomes

$$\Delta\theta = \frac{8\pi^2 b^2 N\Omega_r}{c\lambda},\tag{4.1.15}$$

or, in terms of the total length, $L = 2\pi bN$, of the optical fiber,

$$\Delta\theta = \frac{4\pi Lb\Omega_r}{c\lambda}.\tag{4.1.16}$$

Equation (4.1.16) represents the important result that the phase shift induced by rotation of a Sagnac fiber ring interferometer increases linearly with the total length of the optical fiber.

The second scheme devised to increase the signal from a ring laser gyroscope is the introduction of an active laser medium into the ring cavity. This arrangement is illustrated by Fig. 4.3. For convenience, throughout the rest of this subsection, such an arrangement will be called an active ring laser gyro. Then the CW and CCW ring laser modes have different frequencies because of the difference in effective round-trip optical path lengths caused by the rotation of the cavity. Thus we have only oscillations with frequencies satisfying the resonance condition associated with L_{\pm} corresponding to the effective cavity lengths seen by the CW and CCW propagating beams, respectively, namely

$$v_{\pm} = \frac{m\pi c}{L_{+}},\tag{4.1.17}$$

where m is an integer and

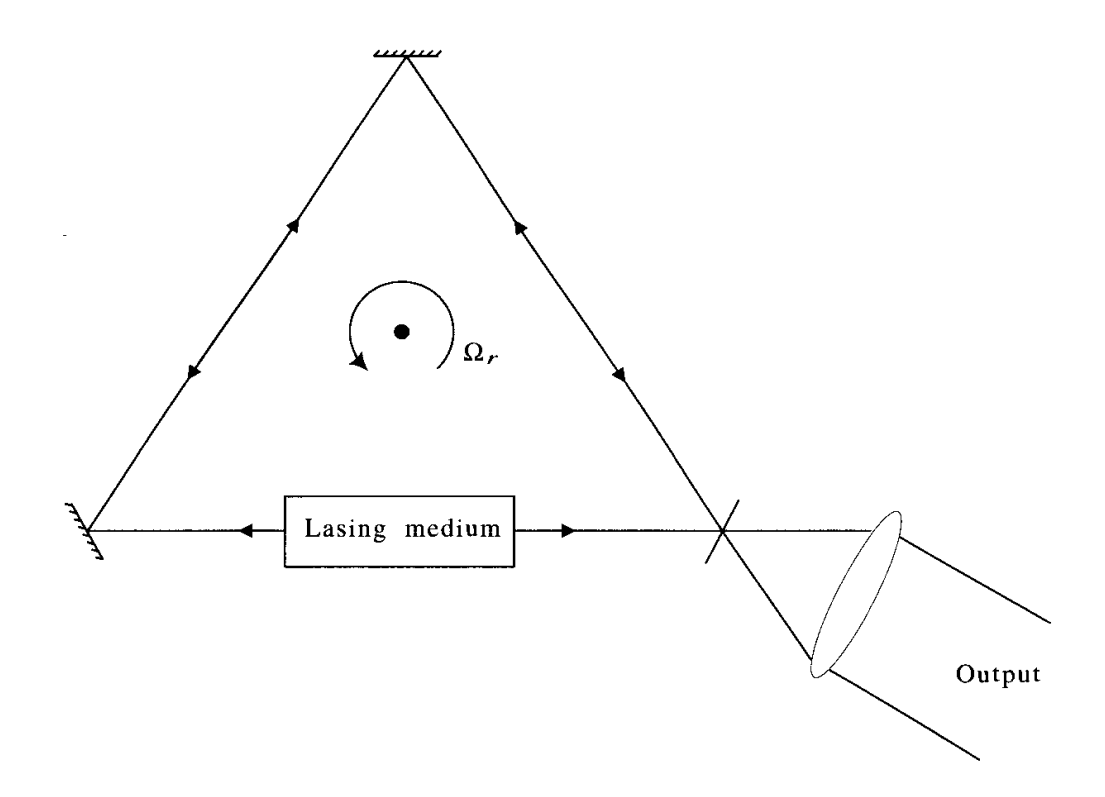
$$L_{\pm} = L \left(1 \pm \frac{b\Omega_r}{c} \right). \tag{4.1.18}$$

Using Eq. (4.1.17) the frequency difference between the CW and CCW propagating beams can be approximated by

$$\Delta v = v_{-} - v_{+} = \frac{m\pi c}{L_{-}} - \frac{m\pi c}{L_{+}} \cong \frac{m\pi c\Delta L}{L^{2}} = v\frac{\Delta L}{L}.$$
 (4.1.19)

The approximation arises out of setting $L_+L_-\cong L^2$.

Fig. 4.3 Schematics of an active ring laser gyroscope.



Now, a couple of important points need to be made. The first of these is that when using an active ring laser gyro it is the frequency difference (not the optical path difference) between the counterpropagating beams which is measured. This frequency difference is generally measured by heterodyning the two output beams. Also note that the frequency difference given by Eq. (4.1.19) is a factor of v/L larger than the optical path length difference given by Eq. (4.1.12). This increased scale factor together with the relative experimental ease associated with small frequency difference measurements makes the active ring laser gyro the most common and, currently, the most sensitive interferometer rotation sensor.

Inserting Eq. (4.1.12) into Eq. (4.1.19) gives (for a circular ring)

$$\Delta v = \frac{2vb\Omega_r}{c} = \frac{2b\Omega_r}{\bar{\lambda}}.$$
 (4.1.20)

Note that Δv does not depend on the total length of the cavity so an increased scale factor is not achieved by using long fiber optic coils in active ring laser gyros. For an arbitrary cavity geometry, Eq. (4.1.20) becomes

$$\Delta v = \frac{4A\Omega_r}{p\bar{\lambda}},\tag{4.1.21}$$

where A is the area enclosed by the light path and p is the perimeter of the light path. The constant of proportionality, $4A/\bar{\lambda}p$, between Δv

and Ω_r is often called the scale factor, which we will later represent by the symbol S.

4.1.3 Proposed ring laser test of metric gravitation theories

Recent progress in research using ring laser gyroscopic devices indicates that rotation rates as slow as $10^{-10} \, \Omega_{\oplus}$, where Ω_{\oplus} is the earth's rotation rate, are potentially measurable. With this in mind, experiments sensitive to Machian frame-dragging (Lense-Thirring effect), the presence of a preferred frame in the universe (preferred frame cosmology), and the curvature of local spacetime can now be envisioned.

Since Einstein formulated the general theory of relativity, there have been many other alternative theories of gravitation, e.g., due to Brans-Dicke and Ni. These theories, which have been motivated by different considerations, lead to different predictions for the effects discussed above. The theoretical framework of the parametrized post-Newtonian (PPN) formalism, which provides a means for studying a very wide class of metric theories of gravitation in the weak-field and slow-motion setting of the solar system, has been developed to systematically compare the various theories with experiment.

When an ultrasensitive ring laser is placed on the rotating earth, we expect to have several 'effective rotations' depending on the particular theory of metric gravity and spacetime we choose. These are summarized in Fig. 4.4 and Table 4.1. There, we see that in addition to the rotation of the ring at $\Omega_{\rm o}$ and the earth's rotation Ω_{\oplus} , we have three other contributions corresponding to $\Omega_{\rm Mach}$, $\Omega_{\rm Cosmos}$, and $\Omega_{\rm Curve}$, respectively.

The first of these effective rotations, Ω_{Mach} , is regarded as a "weak" verification of Mach's principle. That is, our gyro experiences an effective rotation even if it is fixed relative to the fixed stars (i.e., if we step off the earth so that the Ω_{o} and Ω_{\oplus} do not directly affect our ring laser). This effective rotation rate is due solely to the fact that we are near another massive rotating body – the earth. Another way to interpret this is as a kind of magnetic gravity analogous to the magnetic moment associated with a spinning electron.

The second contribution, Ω_{Cosmos} , arises from the presence of a preferred (rest) coordinate system. This 'preferred frame' might be thought to be that implied by the 3 K black-body background. Einstein's theory of general relativity involves no preferred coordinate frame, while in the theory of Ni the universe is at rest in a preferred frame. This effect is especially interesting since it is one of the least well established in gravitation physics.

Table 4.1. Theories of spacetime and effective rotations.

Effective rotation	Physical origin	PPN form	Order of magnitude	Einstein		ï
$\Omega_{ m Mach}$	Mach principle or	$rac{C_1}{8}(7\Delta_1+\Delta_2)\Omega_\oplus$	$5.6 \times 10^{-10} \times \frac{[7\Delta_1 + \Delta_2]}{8} \Omega_{\oplus} \Delta_1 = 1 \Delta_1 = \frac{10 + 7\omega}{14 + 7\omega}$	$\Delta_1 = 1$		$\Delta_1 = \frac{1}{7}$
	magnetic gravity	C_1 depends on latitude etc. and is of order 5.6×10^{-10}	$\Delta_2 = 1$	$\Delta_2 = 1$	$\Delta_2 = 1$ $\omega = \text{number}$ of order 27	$\Delta_2 = 1$
$\Omega_{ m Cosmos}$	Preferred frame or	$rac{C_2}{2}lpha_1\Omega_\oplus$	$1.2 \times 10^{-7} \times \alpha_1 \Omega_{\oplus}$	$\alpha_1 = 0$	$\alpha_2 = 0$	$\alpha_1 = -8$
	motion through the 3 K cosmic black-body background	$\vec{C_2}$ depends on velocity of earth through 3 K background and is of				
$\Omega_{ m Curve}$	Spacetime curvature	order 1.2×10^{-7} $\frac{C_3}{2}(1+\gamma)\Omega_{\oplus}$	$1.4 \times 10^{-9} imes \left\lceil rac{\gamma + 1}{2} ight ceil \Omega_{\oplus}$	$\gamma = 1$	$\gamma = \frac{1+\omega}{2+\omega}$	$\gamma = 1$
		C_3 depends on latitude etc. and is of order 1.4×10^{-9}	7		-	

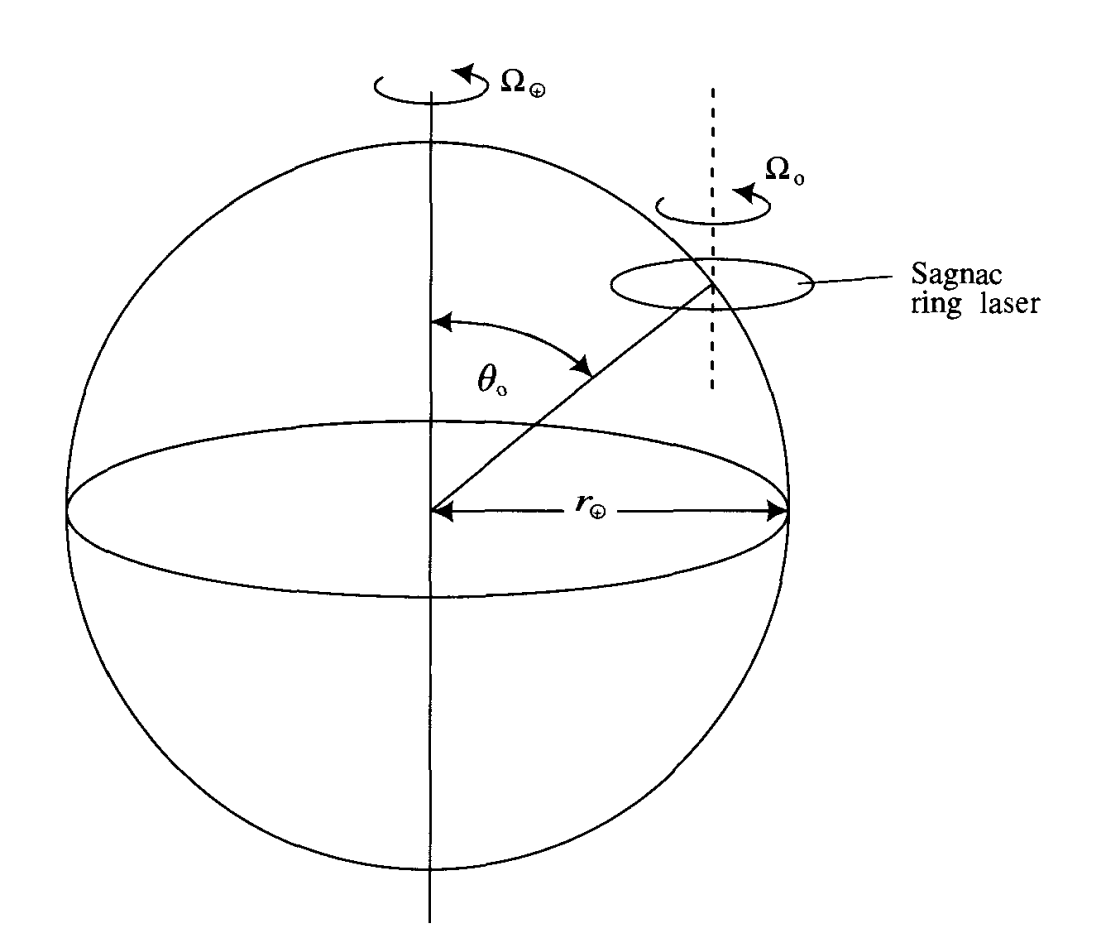


Fig. 4.4
Sagnac ring laser
interferometer used
to test metric theories
of gravity.

The final term, Ω_{Curve} , is due to the fact that we use a curved space metric. Similar 'curved space' physics leads to the bending of starlight and the gravitational red shift, etc.

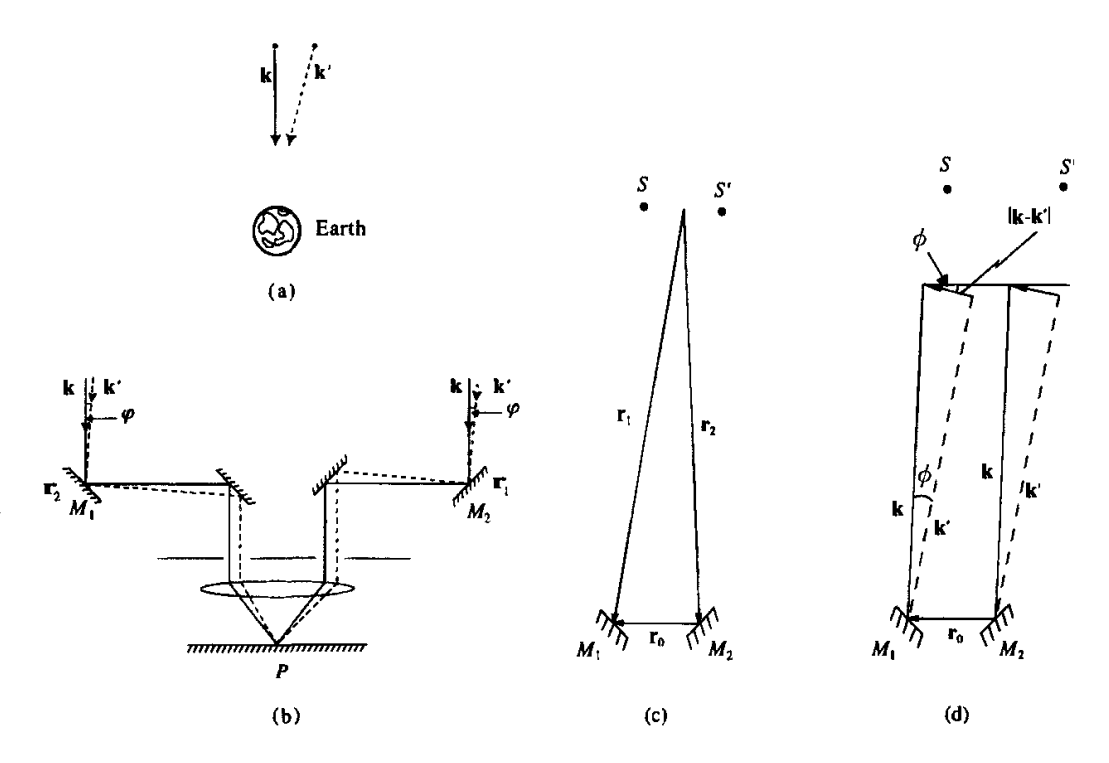
The application of modern quantum optical tools to problems in gravitational physics calls for heroic and imaginative experimental effort. However, it is clear that such effort will yield rich dividends in both fundamental and applied science.

4.1.4 The Michelson stellar interferometer

Consider the simple double (i.e., double source) interference setup as in Fig. 4.5. In Fig. 4.5(a), we see a binary star 'sending' light to earth with wave vectors \mathbf{k} and \mathbf{k}' , and we wish to measure their angular separation, φ .

One way to accomplish this is to collect the light by mirrors M_1 and M_2 , as in Fig. 4.5(b), and to beat the light from two stars on the photodetector located at the point P chosen so that the two paths

Fig. 4.5 (a) A binary star sending light to earth with wave vectors k and k'. (b) Schematics of a Michelson stellar interferometer to measure the angular separation of athe binary star. (c) Filtered light from star S arrives at mirrors M_1 and M_2 with phase factors $\exp(-iv_kt+i\mathbf{k}\cdot\mathbf{r}_1)$ and $\exp(-iv_kt+i\mathbf{k}\cdot\mathbf{r}_2),$ respectively, while that from star S'goes as $\exp(-iv_{k'}t + i\mathbf{k}' \cdot \mathbf{r}_1)$ and $\exp(-iv_{k'}t+i\mathbf{k}'\cdot\mathbf{r}_2).$ (d) Illustration that for small angls, $(\mathbf{k} - \mathbf{k}') \cdot (\mathbf{r}_1 - \mathbf{r}_2) =$ $|\mathbf{k}-\mathbf{k}'|r_0\cos\phi\approx\phi kr_0$ since $|\mathbf{k} - \mathbf{k}'| \simeq k\phi$ and $\cos \phi \simeq 1$.



 $\overline{M_1P}$ and $\overline{M_2P}$ are equal. The photocurrent is then given by

$$I = \kappa \langle E^* E \rangle$$

$$= \kappa \langle |E_{\mathbf{k}}(e^{i\mathbf{k}\cdot\mathbf{r}_1} + e^{i\mathbf{k}\cdot\mathbf{r}_2}) + E_{\mathbf{k}'}(e^{i\mathbf{k}'\cdot\mathbf{r}_1} + e^{i\mathbf{k}'\cdot\mathbf{r}_2})|^2 \rangle$$

$$= \kappa \langle 2(|E_{\mathbf{k}}|^2 + |E_{\mathbf{k}'}|^2) + |E_{\mathbf{k}}|^2 [e^{i\mathbf{k}'\cdot(\mathbf{r}_1 - \mathbf{r}_2)} + \text{c.c.}]$$

$$+ |E_{\mathbf{k}'}|^2 [e^{i\mathbf{k}'\cdot(\mathbf{r}_1 - \mathbf{r}_2)} + \text{c.c.}] \rangle, \tag{4.1.22}$$

where we have made the simplifying assumption that the light from the stars has been filtered so that we may take $v_{\mathbf{k}} = v_{\mathbf{k}'}$ and therefore the temporal factors like $\exp(iv_{\mathbf{k}}t)$ and $\exp(iv_{\mathbf{k}'}t)$ cancel from Eq. (4.1.22). Furthermore, since the radiation from a star is thermal $\langle E_{\mathbf{k}} \rangle = \langle E_{\mathbf{k}'} \rangle = 0$ and $\langle E_{\mathbf{k}}^* E_{\mathbf{k}'} \rangle = \langle E_{\mathbf{k}}^* \rangle \langle E_{\mathbf{k}'} \rangle = 0$. Finally, we note that κ is an uninteresting constant depending of the characteristics of the photodetector and the distance to the star, etc.

If
$$\langle |E_{\mathbf{k}}|^2 \rangle = \langle |E_{\mathbf{k}'}|^2 \rangle = I_0$$
, we have

$$I = 2\kappa I_0 \left\{ 2 + \cos[\mathbf{k} \cdot (\mathbf{r}_1 - \mathbf{r}_2)] + \cos[\mathbf{k}' \cdot (\mathbf{r}_1 - \mathbf{r}_2)] \right\}$$

$$= 4\kappa I_0 \left\{ 1 + \cos[(\mathbf{k} + \mathbf{k}') \cdot (\mathbf{r}_1 - \mathbf{r}_2)/2] \right\}$$

$$\times \cos[(\mathbf{k} - \mathbf{k}') \cdot (\mathbf{r}_1 - \mathbf{r}_2)/2] \right\}. \tag{4.1.23}$$

From Fig. 4.5(d) we see that $(\mathbf{k} - \mathbf{k}') \cdot (\mathbf{r}_1 - \mathbf{r}_2) \cong \varphi k r_0$, so that (4.1.23) may be written as

$$I = 4\kappa I_0 \left\{ 1 + \cos\left[(\mathbf{k} + \mathbf{k}') \cdot (\mathbf{r}_1 - \mathbf{r}_2)/2 \right] \cos\left(\frac{\pi r_0 \varphi}{\lambda}\right) \right\}, \quad (4.1.24)$$

where we have noted $|\mathbf{k}| = |\mathbf{k}'| = 2\pi/\lambda$. Thus, we see that the photocurrent will contain an interference term which is modulated as we vary r_0 and would serve to determine φ varying r_0 until $\pi r_0 \varphi/\lambda = \pi$, etc.

This clever scheme has been applied to several nearby binaries. Unfortunately, atmospheric and instrumental fluctuations enter strongly into the term $\cos \left[(\mathbf{k} + \mathbf{k}') \cdot (\mathbf{r}_1 - \mathbf{r}_2)/2 \right]$ in Eq. (4.1.24) and limit the utility of the approach. This is where Hanbury-Brown and Twiss make their dramatic entrance.

4.1.5 Hanbury-Brown-Twiss interferometer

The essence of the Hanbury-Brown-Twiss (HB-T) stellar interferometer is to recognize that if we consider two photodetectors at points A_1 and A_2 with position vectors \mathbf{r}_1 and \mathbf{r}_2 , respectively, as in Fig. 4.6, then we have the photocurrents

$$I(\mathbf{r}_{i},t) = \kappa \left\{ |E_{\mathbf{k}}|^{2} + |E_{\mathbf{k}'}|^{2} + \left[E_{\mathbf{k}} E_{\mathbf{k}'}^{*} e^{i(\mathbf{k}-\mathbf{k}')\cdot\mathbf{r}_{i}} + \text{c.c.} \right] \right\}$$
 (4.1.25)

and there is phase information in the $\exp[i(\mathbf{k} - \mathbf{k}') \cdot \mathbf{r}_i]$ terms.

What if we multiply the currents from two detectors (at A_1 and A_2 in Fig. 4.6)? From Eq. (4.1.25) this will yield

$$\langle I(\mathbf{r}_{1},t)I(\mathbf{r}_{2},t)\rangle$$

$$= \kappa^{2} \left\langle \left\{ |E_{\mathbf{k}}|^{2} + |E_{\mathbf{k}'}|^{2} + \left[E_{\mathbf{k}} E_{\mathbf{k}'}^{*} e^{i(\mathbf{k}-\mathbf{k}') \cdot \mathbf{r}_{1}} + \text{c.c.} \right] \right\}$$

$$\times \left\{ |E_{\mathbf{k}}|^{2} + |E_{\mathbf{k}'}|^{2} + \left[E_{\mathbf{k}} E_{\mathbf{k}'}^{*} e^{i(\mathbf{k}-\mathbf{k}') \cdot \mathbf{r}_{2}} + \text{c.c.} \right] \right\} \right\rangle$$

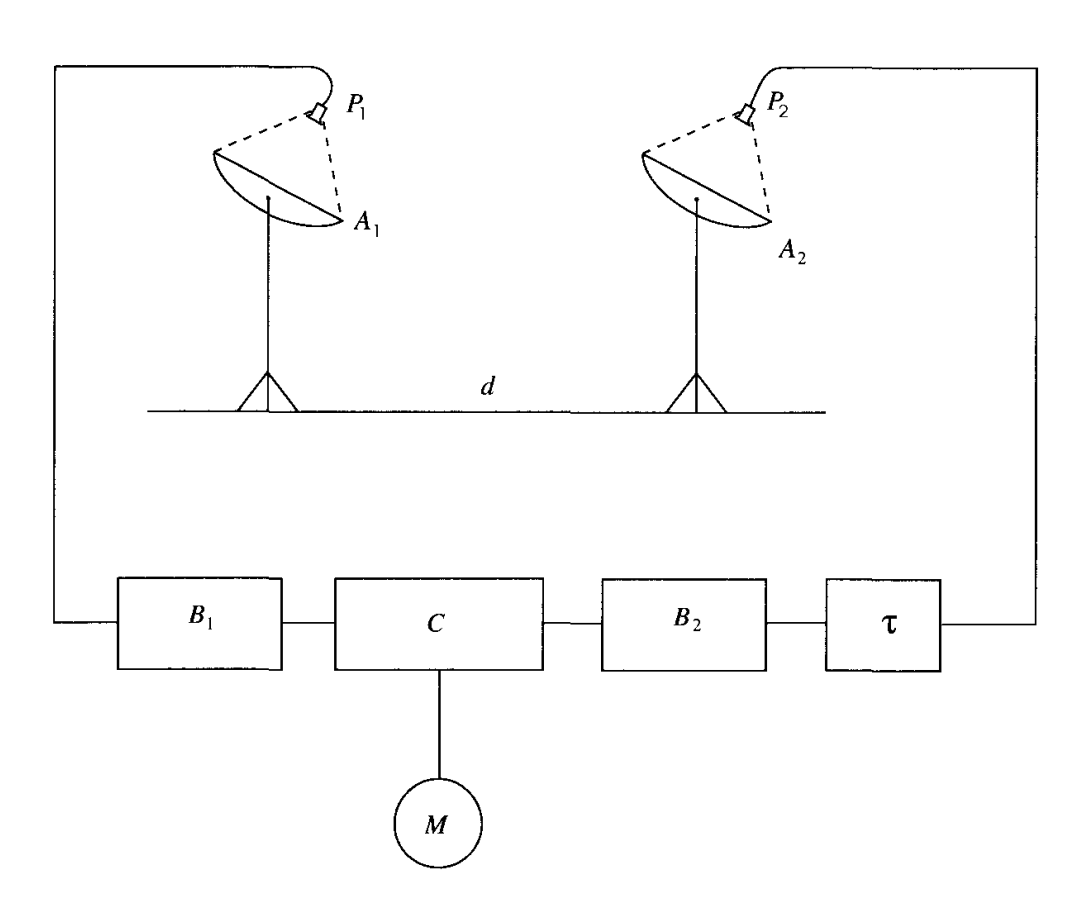
$$= \kappa^{2} \left\{ \left\langle \left(|E_{\mathbf{k}}|^{2} + |E_{\mathbf{k}'}|^{2} \right)^{2} \right\rangle$$

$$+ \left\langle |E_{\mathbf{k}}|^{2} \right\rangle \left\langle |E_{\mathbf{k}'}|^{2} \right\rangle \left[e^{i(\mathbf{k}-\mathbf{k}') \cdot (\mathbf{r}_{1}-\mathbf{r}_{2})} + \text{c.c.} \right] \right\}, \tag{4.1.26}$$

where we have used the fact that $\langle |E_{\bf k}|^2 E_{\bf k}^* E_{\bf k'} \rangle = 0$, etc. Thus we see that the desired low frequency interference term is present; but atmospherically sensitive terms like $\cos[({\bf k}+{\bf k}')\cdot({\bf r}_1-{\bf r}_2)/2]$ are absent. This is the key insight of Hanbury Brown and Twiss.

It is fair to say, however, that the Hanbury-Brown-Twiss effect created quite a stir when it was first announced. Many questions were voiced, e.g., how can we get phase information by beating photocurrents? Does this not somehow violate quantum mechanics? And what about Dirac's statement that photons only interfere with themselves? The confusion is resolved by considering the quantum theory of photon detection and correlation to which we now turn.

Fig. 4.6 Schematic diagram of the Hanbury Brown-Twiss stellar intensity interferometer. Here P_1 and P_2 are the photodetectors, A_1 and A_2 are the mirrors, B_1 and B_2 are the amplifiers, τ is the delay time, C is a multiplier, and M is the integrator.



4.2 Photon detection and quantum coherence functions

A more complete account of photodetection theory is given in Section 6.5. Here we present a heuristic derivation of photodetection and correlation which is sufficient for the present purposes.

As shown in Chapter 1, the field operator $E(\mathbf{r}, t)$ can be separated into the sum of its positive and negative frequency parts

$$\mathbf{E}(\mathbf{r},t) = \mathbf{E}^{(+)}(\mathbf{r},t) + \mathbf{E}^{(-)}(\mathbf{r},t), \tag{4.2.1}$$

where

$$\mathbf{E}^{(+)}(\mathbf{r},t) = \sum_{\mathbf{k}} \hat{\epsilon}_{\mathbf{k}} \mathscr{E}_{\mathbf{k}} a_{\mathbf{k}} e^{-i\nu_{\mathbf{k}}t + i\mathbf{k}\cdot\mathbf{r}}, \tag{4.2.2}$$

$$\mathbf{E}^{(-)}(\mathbf{r},t) = \sum_{\mathbf{k}} \hat{\epsilon}_{\mathbf{k}} \mathscr{E}_{\mathbf{k}} a_{\mathbf{k}}^{\dagger} e^{i\nu_{k}t - i\mathbf{k}\cdot\mathbf{r}}.$$
(4.2.3)

In the following we shall assume, for simplicity, that the field is linearly polarized so that we deal with the scalar quantities $E^{(+)}(\mathbf{r},t) = \hat{\epsilon} \cdot \mathbf{E}^{(+)}(\mathbf{r},t)$ and $E^{(-)}(\mathbf{r},t) = \hat{\epsilon} \cdot \mathbf{E}^{(-)}(\mathbf{r},t)$.

In the optical region, the detectors usually use the photoelectric effect to make local field measurements. Schematically an atom is

placed in the radiation field at position \mathbf{r} in its ground state. The photoelectrons produced by photoionization are then observed. In such absorptive detectors, the measurements are destructive as the photons responsible for producing photoelectrons disappear. In this case, therefore, only the annihilation operator $E^{(+)}$ contributes. The transition probability of the detector atom for absorbing a photon from the field at position \mathbf{r} between times t and t+dt is proportional to $w_1(\mathbf{r},t)dt$, with

$$w_1(\mathbf{r},t) = |\langle f|E^{(+)}(\mathbf{r},t)|i\rangle|^2,$$
 (4.2.4)

where $|i\rangle$ is the initial state of the field before the detection process and $|f\rangle$ is the final state in which the field could be found after the process. The final state of the field is never measured. We can therefore sum over all the final states

$$w_{1}(\mathbf{r},t) = \sum_{f} |\langle f|E^{(+)}(\mathbf{r},t)|i\rangle|^{2}$$

$$= \sum_{f} \langle i|E^{(-)}(\mathbf{r},t)|f\rangle\langle f|E^{(+)}(\mathbf{r},t)|i\rangle$$

$$= \langle i|E^{(-)}(\mathbf{r},t)E^{(+)}(\mathbf{r},t)|i\rangle, \qquad (4.2.5)$$

where in the last line we use the completeness relation

$$\sum_{f} |f\rangle\langle f| = 1. \tag{4.2.6}$$

The photon counting rate w_1 is therefore proportional to the expectation value of the positive definite Hermitian operator $E^{(-)}(\mathbf{r},t)E^{(+)}(\mathbf{r},t)$ taken in the initial state of the field $|i\rangle$. In practice, however, we almost never know precisely the state $|i\rangle$. Since the precise knowledge of the field does not usually exist, we resort to a statistical description by averaging over all the possible realizations of the initial field

$$w_1(\mathbf{r},t) = \sum_{i} P_i \langle i | E^{(-)}(\mathbf{r},t) E^{(+)}(\mathbf{r},t) | i \rangle. \tag{4.2.7}$$

If we introduce the density operator for the field

$$\rho = \sum_{i} P_{i} |i\rangle\langle i|, \tag{4.2.8}$$

we can rewrite Eq. (4.2.7) as

$$w_1(\mathbf{r},t) = \text{Tr}[\rho E^{(-)}(\mathbf{r},t)E^{(+)}(\mathbf{r},t)]. \tag{4.2.9}$$

We define the first-order correlation function of the field

$$G^{(1)}(\mathbf{r}_1, \mathbf{r}_2; t_1, t_2) = \text{Tr}[\rho E^{(-)}(\mathbf{r}_1, t_1) E^{(+)}(\mathbf{r}_2, t_2)]$$

= $\langle E^{(-)}(\mathbf{r}_1, t_1) E^{(+)}(\mathbf{r}_2, t_2) \rangle$. (4.2.10)

Usually we deal with statistically stationary fields in optics, i.e., the correlation functions of the field are invariant under displacements of the time variable. The correlation function $G^{(1)}(\mathbf{r}_1, \mathbf{r}_2; t_1, t_2)$ then depends on t_1 and t_2 only through the time difference $\tau = t_2 - t_1$, i.e.,

$$G^{(1)}(\mathbf{r}_1, \mathbf{r}_2; t_1, t_2) \equiv G^{(1)}(\mathbf{r}_1, \mathbf{r}_2; \tau).$$
 (4.2.11)

In terms of $G^{(1)}$, the counting rate w_1 is given by

$$w_1 = G^{(1)}(\mathbf{r}, \mathbf{r}; 0). \tag{4.2.12}$$

We now consider the joint counting rate at two photodetectors at \mathbf{r}_1 and \mathbf{r}_2 . The joint probability of observing one photoionization at point \mathbf{r}_2 between t_2 and $t_2 + dt_2$ and another one at point \mathbf{r}_1 between t_1 and $t_1 + dt_1$ with $t_1 \le t_2$ is proportional to $w_2(\mathbf{r}_1, t_1; \mathbf{r}_2, t_2)dt_1dt_2$, where

$$w_2(\mathbf{r}_1, t_1; \mathbf{r}_2, t_2) = |\langle f|E^{(+)}(\mathbf{r}_2, t_2)E^{(+)}(\mathbf{r}_1, t_1)|i\rangle|^2. \tag{4.2.13}$$

It follows, on summing over all the final states and averaging over all the possible realizations of the initial field as before, that

$$w_2(\mathbf{r}_1, t_1; \mathbf{r}_2, t_2) = \text{Tr}[\rho E^{(-)}(\mathbf{r}_1, t_1) E^{(-)}(\mathbf{r}_2, t_2) E^{(+)}(\mathbf{r}_2, t_2) E^{(+)}(\mathbf{r}_1, t_1)].$$
(4.2.14)

The joint probability of photodetection is thus governed by the secondorder quantum mechanical correlation function

$$G^{(2)}(\mathbf{r}_{1}, \mathbf{r}_{2}, \mathbf{r}_{3}, \mathbf{r}_{4}; t_{1}, t_{2}, t_{3}, t_{4}) = \operatorname{Tr}[\rho E^{(-)}(\mathbf{r}_{1}, t_{1}) E^{(-)}(\mathbf{r}_{2}, t_{2}) \times E^{(+)}(\mathbf{r}_{3}, t_{3}) E^{(+)}(\mathbf{r}_{4}, t_{4})]$$

$$= \langle E^{(-)}(\mathbf{r}_{1}, t_{1}) E^{(-)}(\mathbf{r}_{2}, t_{2}) \times E^{(+)}(\mathbf{r}_{3}, t_{3}) E^{(+)}(\mathbf{r}_{4}, t_{4}) \rangle. \quad (4.2.15)$$

In general, we can define the *n*th-order correlation function

$$G^{(n)}(\mathbf{r}_{1},...,\mathbf{r}_{n},\mathbf{r}_{n+1},...,\mathbf{r}_{2n};t_{1},...,t_{n},t_{n+1},...,t_{2n})$$

$$= \operatorname{Tr}[\rho E^{(-)}(\mathbf{r}_{1},t_{1})...E^{(-)}(\mathbf{r}_{n},t_{n})E^{(+)}(\mathbf{r}_{n+1},t_{n+1})...E^{(+)}(\mathbf{r}_{2n},t_{2n})]$$

$$= \langle E^{(-)}(\mathbf{r}_{1},t_{1})...E^{(-)}(\mathbf{r}_{n},t_{n})E^{(+)}(\mathbf{r}_{n+1},t_{n+1})...E^{(+)}(\mathbf{r}_{2n},t_{2n})\rangle.$$
(4.2.16)

In this definition of the nth-order correlation function we have included

equal numbers of creation and destruction operators because such correlation functions are measured in typical multi-photon counting experiments.

It is apparent from the above discussion that the correlation functions of the field operators which are encountered in any photon detection experiment based on the photoelectric effect are in normal order (that is, with all the destruction operators on the right and all the creation operators on the left). For example, the average light intensity at point \mathbf{r} at time t is

$$\langle I(\mathbf{r},t)\rangle = \langle E^{(-)}(\mathbf{r},t)E^{(+)}(\mathbf{r},t)\rangle,\tag{4.2.17}$$

and the measured intensity-intensity correlation function is equal to $\langle E^{(-)}(\mathbf{r},t)E^{(-)}(\mathbf{r},t)E^{(+)}(\mathbf{r},t)E^{(+)}(\mathbf{r},t)\rangle$, which is different from $\langle I(\mathbf{r},t)I(\mathbf{r},t)\rangle$.

We can define the quantum mechanical first- and second-order degrees of coherence at the position \mathbf{r} as

$$g^{(1)}(\mathbf{r},\tau) = \frac{\langle E^{(-)}(\mathbf{r},t)E^{(+)}(\mathbf{r},t+\tau)\rangle}{\sqrt{\langle E^{(-)}(\mathbf{r},t)E^{(+)}(\mathbf{r},t)\rangle\langle E^{(-)}(\mathbf{r},t+\tau)E^{(+)}(\mathbf{r},t+\tau)\rangle}}, \quad (4.2.18)$$

$$g^{(2)}(\mathbf{r},\tau) = \frac{\langle E^{(-)}(\mathbf{r},t)E^{(-)}(\mathbf{r},t+\tau)E^{(+)}(\mathbf{r},t+\tau)E^{(+)}(\mathbf{r},t)\rangle}{\langle E^{(-)}(\mathbf{r},t)E^{(+)}(\mathbf{r},t)\rangle\langle E^{(-)}(\mathbf{r},t+\tau)E^{(+)}(\mathbf{r},t+\tau)\rangle}, \quad (4.2.19)$$

where we have assumed the field to be statistically stationary. In the definition of $g^{(2)}(\mathbf{r},\tau)$, we have chosen not only the normal ordering of the field operators in the numerator but a certain time ordering. This time ordering is a consequence of the way the photoelectron rate is calculated above (note that $t_2 \geq t_1$ in Eq. (4.2.14)). Considerably simpler forms for these quantities are obtained in the special case when the radiation field consists of only a single mode. Then most factors cancel when the mode expansions for $E^{(+)}$ and $E^{(-)}$ are substituted from Eqs. (4.2.2) and (4.2.3) into Eqs. (4.2.18) and (4.2.19), leaving

$$g^{(1)}(\tau) = \frac{\langle a^{\dagger}(t)a(t+\tau)\rangle}{\langle a^{\dagger}a\rangle},\tag{4.2.20}$$

$$g^{(2)}(\tau) = \frac{\langle a^{\dagger}(t)a^{\dagger}(t+\tau)a(t+\tau)a(t)\rangle}{\langle a^{\dagger}a\rangle^2}.$$
 (4.2.21)

Since only the normally ordered correlation functions are involved in the photodetection processes, the P-representation $P(\alpha, \alpha^*)$ forms a correspondence between classical and quantum coherence theory. This happens because the quantum mechanical expectation values

of the normally ordered functions can be calculated from the *P*-representation just as we would evaluate the corresponding classical coherence function from a classical distribution function. The *P*-representation, however, does not have all the properties of a classical distribution function. In particular, as discussed in Section 3.1, the *P*-representation is not nonnegative definite. Light fields for which the *P*-representation is not a well-behaved distribution will exhibit nonclassical features of light. We will discuss some of them in Section 4.4.

We now derive the normalized correlation function $g^{(2)}(\tau)$ for thermal and coherent fields within the framework of the quantum theory of coherence. The *P*-representation of a single-mode thermal field is given by a Gaussian distribution (Eq. (3.1.26)):

$$P(\alpha, \alpha^*) = \frac{1}{\pi \langle n \rangle} \exp(-|\alpha|^2 / \langle n \rangle). \tag{4.2.22}$$

We then have

$$g^{(2)}(0) = \frac{\int P(\alpha, \alpha^*) |\alpha|^4 d^2 \alpha}{\left[\int P(\alpha, \alpha^*) |\alpha|^2 d^2 \alpha\right]^2} = 2.$$
 (4.2.23)

However, for a laser operating far above threshold, the field is in a coherent state $|\alpha_0\rangle$, for which (see Eq. (3.1.28))

$$P(\alpha, \alpha^*) = \delta^{(2)}(\alpha - \alpha_0). \tag{4.2.24}$$

The normalized correlation then is

$$g^{(2)}(0) = 1. (4.2.25)$$

4.3 First-order coherence and Young-type double-source experiments

4.3.1 Young's double-slit experiment

One of the classic experiments that exhibits the first-order coherence properties of light is Young's double-slit experiment (see Fig. 4.7). The complex field generated by a quasimonochromatic light source is split at the screen S_1 by placing an opaque screen across the beam with pinholes at points P_1 and P_2 . The positive frequency part of the field operator at a point P on the screen S_2 at time t may be approximated by a linear superposition of the field operators present at P_1 and P_2 at earlier times:

$$E^{(+)}(\mathbf{r},t) = K_1 E^{(+)}(\mathbf{r}_1, t - t_1) + K_2 E^{(+)}(\mathbf{r}_2, t - t_2), \tag{4.3.1}$$

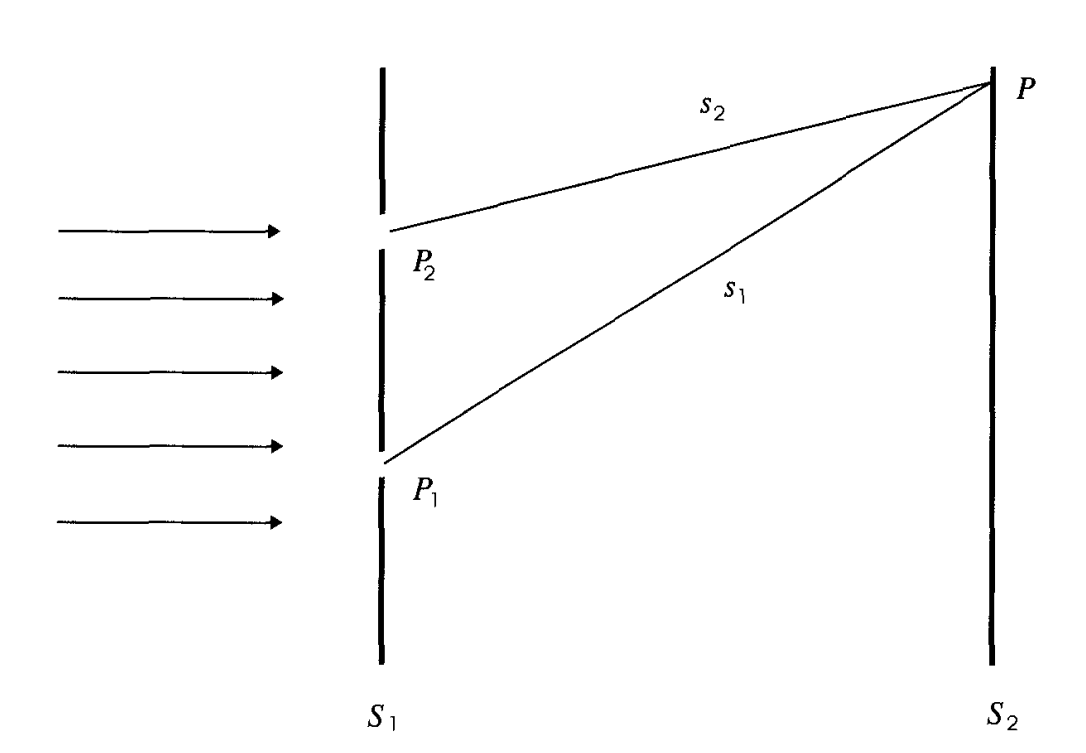


Fig. 4.7 Schematic diagram of an idealized Young's double-slit experiment.

where $t_i = s_i/c$ (i = 1, 2) is the time needed for the light to travel from the pinhole P_i to the point P and \mathbf{r}_1 and \mathbf{r}_2 are the position vectors at the pinholes P_1 and P_2 , respectively. The coefficients K_1 and K_2 depend on the size and geometry of the pinholes. From diffraction theory it follows that K_1 and K_2 are purely imaginary numbers.

A photodetector placed at the point P measures the intensity

$$\langle I(\mathbf{r},t)\rangle = \text{Tr}[\rho E^{(-)}(\mathbf{r},t)E^{(+)}(\mathbf{r},t)]$$

$$= |K_1|^2 \text{Tr}[\rho E^{(-)}(\mathbf{r}_1,t-t_1)E^{(+)}(\mathbf{r}_1,t-t_1)]$$

$$+ |K_2|^2 \text{Tr}[\rho E^{(-)}(\mathbf{r}_2,t-t_2)E^{(+)}(\mathbf{r}_2,t-t_2)]$$

$$+ 2\text{Re}\{K_1^* K_2 \text{Tr}[\rho E^{(-)}(\mathbf{r}_1,t-t_1)E^{(+)}(\mathbf{r}_2,t-t_2)]\}.(4.3.2)$$

We can rewrite this equation in terms of the first-order correlation function

 $G^{(1)}(\mathbf{r}_1,\mathbf{r}_2;t_1,t_2)$ in the following way:

$$\langle I(\mathbf{r},t)\rangle = |K_1|^2 G^{(1)}(\mathbf{r}_1,\mathbf{r}_1;t-t_1,t-t_1) + |K_2|^2 G^{(1)}(\mathbf{r}_2,\mathbf{r}_2;t-t_2,t-t_2) + 2\operatorname{Re}[K_1^* K_2 G^{(1)}(\mathbf{r}_1,\mathbf{r}_2;t-t_1,t-t_2)].$$
(4.3.3)

For statistically stationary fields, expression (4.3.3) for the average intensity at the point P becomes

$$\langle I(\mathbf{r},t)\rangle = |K_1|^2 G^{(1)}(\mathbf{r}_1,\mathbf{r}_1;0) + |K_2|^2 G^{(1)}(\mathbf{r}_2,\mathbf{r}_2;0) +2\operatorname{Re}[K_1^* K_2 G^{(1)}(\mathbf{r}_1,\mathbf{r}_2;\tau)],$$
(4.3.4)

where $\tau = t_1 - t_2$. The average intensity $\langle I(\mathbf{r}, t) \rangle$ is therefore independent of the time t.

The first two terms in Eq. (4.3.4) represent the average intensities at the point P due to the light field at the pinholes P_1 and P_2 , respectively. The last term, however, gives a contribution due to fields at both the pinholes and is responsible for the interference. In order to see this clearly we set

$$\langle I^{(i)}(\mathbf{r})\rangle = |K_i|^2 G^{(1)}(\mathbf{r}_i, \mathbf{r}_i; 0) \qquad (i = 1, 2).$$
 (4.3.5)

We next define the normalized first-order correlation function

$$g^{(1)}(\mathbf{r}_1, \mathbf{r}_2; \tau) = \frac{G^{(1)}(\mathbf{r}_1, \mathbf{r}_2; \tau)}{\sqrt{G^{(1)}(\mathbf{r}_1, \mathbf{r}_1; 0)G^{(1)}(\mathbf{r}_2, \mathbf{r}_2; 0)}}.$$
 (4.3.6)

In terms of $g^{(1)}(\mathbf{r}_1, \mathbf{r}_2; \tau)$, Eq. (4.3.4) can be rewritten as

$$\langle I(\mathbf{r},t)\rangle = \langle I^{(1)}(\mathbf{r})\rangle + \langle I^{(2)}(\mathbf{r})\rangle +2[\langle I^{(1)}(\mathbf{r})\rangle \langle I^{(2)}(\mathbf{r})\rangle]^{1/2} \operatorname{Re}[g^{(1)}(\mathbf{r}_1,\mathbf{r}_2;\tau)].$$
(4.3.7)

Next we set

$$g^{(1)}(\mathbf{r}_1, \mathbf{r}_2; \tau) = |g^{(1)}(\mathbf{r}_1, \mathbf{r}_2; \tau)| e^{i\alpha(\mathbf{r}_1, \mathbf{r}_2; \tau) - i\nu_0 \tau}, \tag{4.3.8}$$

where $\alpha(\mathbf{r}_1, \mathbf{r}_2; \tau) = \arg[g^{(1)}(\mathbf{r}_1, \mathbf{r}_2; \tau)] + v_0 \tau$ and v_0 is the field frequency. We then obtain

$$\langle I(\mathbf{r},t)\rangle = \langle I^{(1)}(\mathbf{r})\rangle + \langle I^{(2)}(\mathbf{r})\rangle + 2[\langle I^{(1)}(\mathbf{r})\rangle\langle I^{(2)}(\mathbf{r})\rangle]^{1/2} \times |g^{(1)}(\mathbf{r}_1,\mathbf{r}_2;\tau)|\cos[\alpha(\mathbf{r}_1,\mathbf{r}_2;\tau) - \nu_0\tau].$$
(4.3.9)

For a quasimonochromatic source of light, $\langle I^{(1)}(\mathbf{r})\rangle$, $\langle I^{(2)}(\mathbf{r})\rangle$, $|g^{(1)}(\mathbf{r}_1,\mathbf{r}_2;\tau)|$, and $\alpha(\mathbf{r}_1,\mathbf{r}_2;\tau)$ vary slowly with respect to position on the screen. However, the cosine term varies rapidly due to the term $v_0\tau = v_0(s_1-s_2)/c$ and will lead to sinusoidal variation of intensity on the screen.

The physical meaning of $g^{(1)}(\mathbf{r}_1, \mathbf{r}_2; \tau)$ can be understood if we consider the visibility of the interference fringes on the screen. The visibility, which is a measure of the sharpness of the interference fringes, is defined as

$$U = \frac{\langle I(\mathbf{r})\rangle_{\text{max}} - \langle I(\mathbf{r})\rangle_{\text{min}}}{\langle I(\mathbf{r})\rangle_{\text{max}} + \langle I(\mathbf{r})\rangle_{\text{min}}},$$
(4.3.10)

where $\langle I(\mathbf{r})\rangle_{\text{max}}$ and $\langle I(\mathbf{r})\rangle_{\text{min}}$ represent the maximum and minimum average intensity, respectively, in the neighborhood of the point P. To a good approximation for $\cos[\alpha(\mathbf{r}_1, \mathbf{r}_2; \tau) - \nu_0 \tau]$ they are equal to +1 and -1 in Eq. (4.3.9). We then obtain

$$U = \frac{2[\langle I^{(1)}(\mathbf{r})\rangle\langle I^{(2)}(\mathbf{r})\rangle]^{1/2}}{\langle I^{(1)}(\mathbf{r})\rangle + \langle I^{(2)}(\mathbf{r})\rangle} |g^{(1)}(\mathbf{r}_1, \mathbf{r}_2; \tau)|, \tag{4.3.11}$$

i.e., the visibility of the fringes is proportional to the magnitude of $g^{(1)}(\mathbf{r}_1,\mathbf{r}_2;\tau)$, which is called the complex degree of coherence. In particular, when the averaged intensities of the two beams are equal, $\langle I^{(1)}(\mathbf{r}) \rangle = \langle I^{(2)}(\mathbf{r}) \rangle$, the visibility U is equal to $|g^{(1)}(\mathbf{r}_1,\mathbf{r}_2;\tau)|$. Thus when $g^{(1)}(\mathbf{r}_1,\mathbf{r}_2;\tau)=0$, no interference fringes are formed in the region around P and it would be implied that the two light beams reaching the point P are mutually incoherent. A maximum visibility of the fringes is obtained around P when $|g^{(1)}(\mathbf{r}_1,\mathbf{r}_2;\tau)|=1$ and the two light beams reaching P are mutually completely coherent. This happens when

$$\langle E^{(-)}(\mathbf{r}_1, t)E^{(+)}(\mathbf{r}_2, t+\tau)\rangle = \mathscr{E}^*(\mathbf{r}_1, t)\mathscr{E}(\mathbf{r}_2, t+\tau). \tag{4.3.12}$$

The intermediate cases $0 < |g^{(1)}(\mathbf{r}_1, \mathbf{r}_2; \tau)| < 1$ characterize partial coherence.

As an example, the emission from a Doppler-broadened spectral light source, such as that from a thermal lamp, is described by

$$G^{(1)}(\mathbf{r}_1, \mathbf{r}_2; \tau) = \mathcal{E}_0^2 \exp(-i\nu_0 \tau - \tau^2 / 2\tau_c^2), \tag{4.3.13}$$

where τ_c is a constant. It is therefore clear that as the path difference $c\tau$ becomes much larger than $c\tau_c$, $|g^{(1)}(\mathbf{r}_1,\mathbf{r}_2;\tau)| = \exp(-\tau^2/2\tau_c^2)$ goes to zero and the interference fringes disappear. The constant τ_c , which will be related to the light bandwidth (shown below), is thus a measure of the coherence time of the light.

An important property of the first-order correlation function

$$G^{(1)}(\mathbf{r},\mathbf{r};\tau) = \langle E^{(-)}(\mathbf{r},t)E^{(+)}(\mathbf{r},t+\tau)\rangle$$

is that it forms a Fourier transform pair with the power spectrum $S(\mathbf{r}, v)$ of the statistically stationary field at the position \mathbf{r} , i.e.,

$$S(\mathbf{r}, v) = \frac{1}{\pi} \operatorname{Re} \int_0^\infty d\tau G^{(1)}(\mathbf{r}, \mathbf{r}; \tau) e^{iv\tau}.$$
 (4.3.14)

We therefore need the first-order correlation function at positive τ to compute the power spectrum.

We consider the example of the Doppler-broadened spectral light source whose first-order correlation function is given by Eq. (4.3.13). The power spectrum for the light source, as computed from Eq. (4.3.14) is therefore equal to

$$S(\mathbf{r}, v) = \frac{\mathscr{E}_0^2 \tau_c}{\sqrt{2\pi}} \exp[-(v - v_0)^2 \tau_c^2 / 2].$$
 (4.3.15)

This is a Gaussian spectrum centered around $v = v_0$ with a full-width at half-maximum equal to $2\sqrt{2\ln 2}/\tau_c$. Thus $1/\tau_c$, which is the inverse of the coherence time of the light field, is a measure of the light bandwidth.

4.3.2 Young's experiment with light from two atoms*

Consider the Young-type experiment shown in Fig. 4.8. There we see two atoms at locations S and S'. At t=0 both atoms are allowed to interact with a single photon, designated by $|\phi\rangle$, and one or other of the atoms may be excited. In this way we prepare the state

$$\alpha (|a,b'\rangle + |b,a'\rangle) |0\rangle + \beta |b,b'\rangle |\phi\rangle, \tag{4.3.16}$$

where $|a\rangle$, $|b\rangle$, and $|a'\rangle$, $|b'\rangle$ denote the excited and ground states of atoms at S and S', and α and β are the probability amplitudes for the states associated with excited and ground state atoms, respectively. Thus, with a probability $|\alpha|^2$ we have prepared the state

$$|\psi(0)\rangle = \frac{1}{\sqrt{2}}(|a,b'\rangle + |b,a'\rangle)|0\rangle \tag{4.3.17}$$

by single-photon absorption. Later in time, this state will decay into the state

$$|\psi(\infty)\rangle = \frac{1}{\sqrt{2}}|b,b'\rangle(|\gamma\rangle + |\gamma'\rangle),$$
 (4.3.18)

where $|\gamma\rangle$ and $|\gamma'\rangle$ denote the photon states associated with emission from sites S and S'. For present purposes, it will suffice to take $|\gamma\rangle$ and $|\gamma'\rangle$ as plane wave states $|1_{\bf k}\rangle$ and $|1_{\bf k'}\rangle$ where ${\bf k}/k$ and ${\bf k'}/k'$ are the unit vectors from S and S' to the detectors at **r**, see Fig. 4.8. However, the question of how to most simply choose the states $|\gamma\rangle$ and $|\gamma'\rangle$ while still being faithful to the physics is an important and subtle one, and is treated in Appendix 4.A.*

The correlation function $G^{(1)}(\mathbf{r},\mathbf{r};t,t)$ now takes the form

$$G^{(1)}(\mathbf{r}, \mathbf{r}; t, t) = \langle \psi(\infty) | E^{(-)}(\mathbf{r}) E^{(+)}(\mathbf{r}) | \psi(\infty) \rangle = G^{(1)}(\mathbf{r}, \mathbf{r}; 0),$$
(4.3.19)

where we have noted that the time-dependent factors cancel because $v_k = v_{k'}$. By completeness as in Eq. (1.5.16), this may be written as

$$G^{(1)}(\mathbf{r}, \mathbf{r}; 0) = \Psi_{\mathscr{E}}^{*}(\mathbf{r})\Psi_{\mathscr{E}}(\mathbf{r}), \tag{4.3.20}$$

^{*} See Scully and Drühl, Phys. Rev. A 25, 2208 (1982).

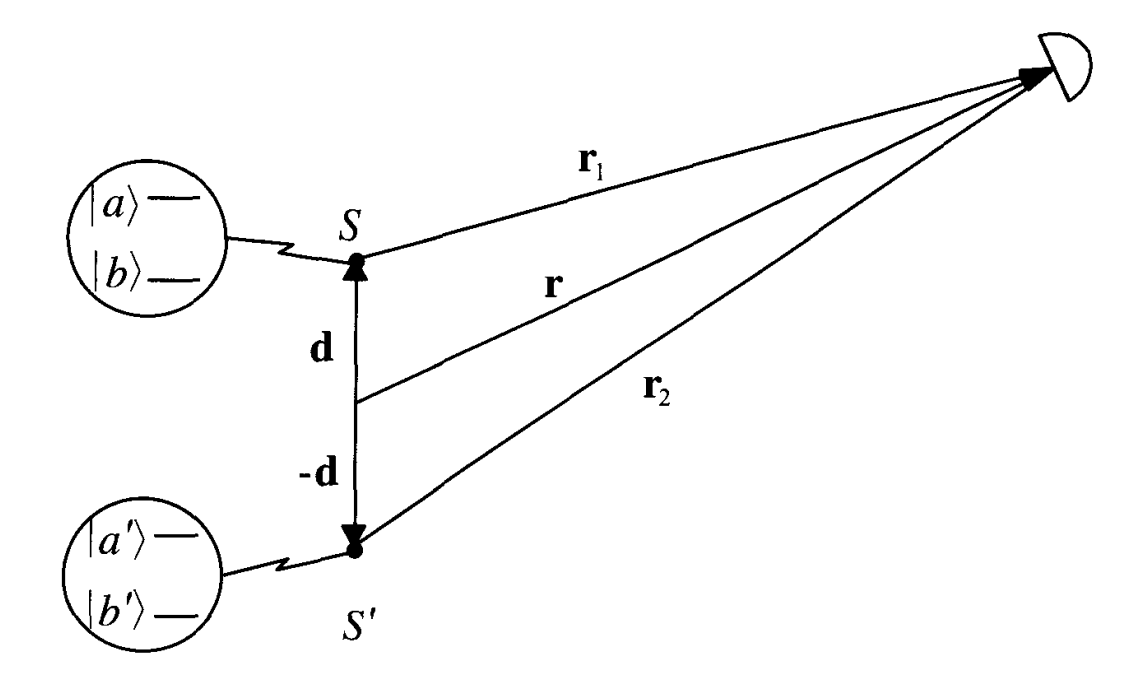


Fig. 4.8 Schematic diagram of an Young-type experiment via light from two atoms.

where

$$\Psi_{\mathscr{E}}(\mathbf{r}) = \langle 0|E^{(+)}(\mathbf{r})|\psi(\infty)\rangle$$

$$= \frac{\mathscr{E}_{\mathbf{k}}}{\sqrt{2}} \left(e^{i\mathbf{k}\cdot\mathbf{r}} + e^{i\mathbf{k}'\cdot\mathbf{r}} \right). \tag{4.3.21}$$

Thus we see that an interference pattern is obtained which is governed by

$$G^{(1)}(\mathbf{r}, \mathbf{r}; 0) = \mathscr{E}_{\mathbf{k}}^{2} \{ 1 + \cos[(\mathbf{k} - \mathbf{k}') \cdot \mathbf{r}] \}, \tag{4.3.22}$$

and as is discussed in Appendix 4.A, this can be written as

$$G^{(1)}(\mathbf{r}, \mathbf{r}; 0) = \mathscr{E}_{\mathbf{k}}^{2} \left[1 + \cos\left(\frac{2k}{r}\mathbf{d} \cdot \mathbf{r}\right) \right]$$
$$= \mathscr{E}_{\mathbf{k}}^{2} \left[1 + \cos(2kxd/D) \right], \tag{4.3.23}$$

which is the usual result.

4.4 Second-order coherence

In the previous section we considered the first-order correlation functions and their properties. For fields with identical spectral properties, it is not possible to distinguish the nature of the light source from only the first-order correlation function. For example, a laser beam and the light generated by a conventional thermal source can both have the same first-order coherence properties. The same, however, is not true when we consider the second- and higher-order coherence properties of the light sources. We therefore turn to the applications of the second-order correlation functions of the field.

4.4.1 The physics behind the Hanbury-Brown-Twiss effect

Armed with a theory of photoelectron correlations, we now return to the Hanbury-Brown-Twiss effect. Let us begin by considering the state $|\psi\rangle = |1_{\bf k}, 1_{\bf k'}\rangle$, i.e., the case of two independent photons one having momentum $\bf k$ and one having momentum $\bf k'$. Now it is clear that the second-order correlation function may be written as

$$G^{(2)}(\mathbf{r}_{1}, \mathbf{r}_{2}; t, t) = \langle 1_{\mathbf{k}}, 1_{\mathbf{k}'} | E^{(-)}(\mathbf{r}_{1}, t) E^{(-)}(\mathbf{r}_{2}, t) E^{(+)}(\mathbf{r}_{2}, t) E^{(+)}(\mathbf{r}_{1}, t) | 1_{\mathbf{k}}, 1_{\mathbf{k}'} \rangle, (4.4.1)$$

and using $\sum_{\{n\}} |\{n\}\rangle\langle\{n\}| = 1$ this becomes

$$G^{(2)}(\mathbf{r}_{1}, \mathbf{r}_{2}; t, t) = \sum_{\{n\}} \langle 1_{\mathbf{k}}, 1_{\mathbf{k}'} | E^{(-)}(\mathbf{r}_{1}, t) E^{(-)}(\mathbf{r}_{2}, t) | \{n\} \rangle$$

$$\times \langle \{n\} | E^{(+)}(\mathbf{r}_{2}, t) E^{(+)}(\mathbf{r}_{1}, t) | 1_{\mathbf{k}}, 1_{\mathbf{k}'} \rangle. \tag{4.4.2}$$

As $|1_{\mathbf{k}}, 1_{\mathbf{k}'}\rangle$ is a two-photon state which is annihilated by $E^{(+)}(\mathbf{r_2}, t)$ $E^{(+)}(\mathbf{r_1}, t)$, only the $|0\rangle\langle 0|$ term survives.

In view of the above, we see that for the case of two single photons we may write

$$G^{(2)}(\mathbf{r}_1, \mathbf{r}_2; t, t) = \Psi^{(2)*}(\mathbf{r}_1, \mathbf{r}_2; t, t)\Psi^{(2)}(\mathbf{r}_1, t; \mathbf{r}_2, t), \tag{4.4.3}$$

where

$$\Psi^{(2)}(\mathbf{r}_1, t; \mathbf{r}_2, t) = \langle 0|E^{(+)}(\mathbf{r}_2, t)E^{(+)}(\mathbf{r}_1, t)|1_{\mathbf{k}}, 1_{\mathbf{k}'}\rangle. \tag{4.4.4}$$

From

$$E^{(+)}(\mathbf{r}_i,t) = \mathscr{E}_{\mathbf{k}} \left(a_{\mathbf{k}} e^{-i\nu t + i\mathbf{k}\cdot\mathbf{r}_i} + a_{\mathbf{k}'} e^{-i\nu t + i\mathbf{k}'\cdot\mathbf{r}_i} \right) \quad (i = 1,2), (4.4.5)$$

these become

$$\Psi^{(2)}(\mathbf{r}_{1}, t; \mathbf{r}_{2}, t) = \mathscr{E}_{\mathbf{k}}^{2} e^{-2i\nu t} \langle 0 | a_{\mathbf{k}} e^{i\mathbf{k}\cdot\mathbf{r}_{1}} a_{\mathbf{k}'} e^{i\mathbf{k}'\cdot\mathbf{r}_{2}} | 1_{\mathbf{k}}, 1_{\mathbf{k}'} \rangle
+ \mathscr{E}_{\mathbf{k}}^{2} e^{-2i\nu t} \langle 0 | a_{\mathbf{k}'} e^{i\mathbf{k}'\cdot\mathbf{r}_{1}} a_{\mathbf{k}} e^{i\mathbf{k}\cdot\mathbf{r}_{2}} | 1_{\mathbf{k}}, 1_{\mathbf{k}'} \rangle
= \mathscr{E}_{\mathbf{k}}^{2} e^{-2i\nu t} \left(e^{i\mathbf{k}\cdot\mathbf{r}_{1}+\mathbf{k}'\cdot\mathbf{r}_{2}} + e^{i\mathbf{k}'\cdot\mathbf{r}_{1}+\mathbf{k}\cdot\mathbf{r}_{2}} \right),$$
(4.4.6)

and

$$G^{(2)}(\mathbf{r}_1, \mathbf{r}_2; t, t) = 2\mathscr{E}_{\mathbf{k}}^4 \left\{ 1 + \cos[(\mathbf{k} - \mathbf{k}') \cdot (\mathbf{r}_1 - \mathbf{r}_2)] \right\}. \tag{4.4.7}$$

$$\Psi^{(2)}(\mathbf{r}_1,\mathbf{r}_2;t,t) = \frac{S}{S'} \frac{1}{2} + \frac{S}{S'} \frac{1}{2}$$

Fig. 4.9 Pictorial representation of terms in Eq. (4.4.6).

PHOTON-CORRELATION INTERFEROMETRY FROM TWO ATOMS

Consider next the case of two atoms at S and S' as in Fig. 4.9 in which both atoms are initially excited, that is,

$$|\psi(0)\rangle = |a, a'\rangle|0\rangle. \tag{4.4.8}$$

Then after many decay times this goes into

$$|\psi(\infty)\rangle = |b, b'\rangle|\gamma, \gamma'\rangle,\tag{4.4.9}$$

where, as in the previous section, we may take $|\gamma\rangle = |1_{\mathbf{k}}\rangle$, $|\gamma'\rangle = |1_{\mathbf{k}'}\rangle$. The two-photon correlation function is then identical with that given by Eqs. (4.4.1) and (4.4.7).

Next we turn to incoherent atom excitation in order to display the real power of the HB-T effect. Specifically, suppose we excite the atoms at S and S' by electron impact. Then at some instant, call it t=0, we will have a state of the form

$$|\psi(0)\rangle = \left[|\alpha|e^{i\varphi}|a,a'\rangle + |\beta| \left(e^{i\theta}|a,b'\rangle + e^{i\theta'}|b,a'\rangle \right) + |\gamma||b,b'\rangle \right] \otimes |0\rangle, \tag{4.4.10}$$

which, see Appendix 4.A for a discussion of the spherical-versus planewave description of interference physics, evolves into

$$|\psi(\infty)\rangle = \left[|\alpha|e^{i\varphi}|1_{\mathbf{k}}, 1_{\mathbf{k}'}\rangle + |\beta| \left(e^{i\theta}|1_{\mathbf{k}}\rangle + e^{i\theta'}|1_{\mathbf{k}'}\rangle \right) + |\gamma||0\rangle \right]$$

$$\otimes |b, b'\rangle, \tag{4.4.11}$$

where φ , θ , and θ' are random phases due, for example, to random excitation times of the atoms.

In such a case, the interference terms in the first-order correlation function will be multiplied by a random phase factor, which we must average over, that is

$$[G^{(1)}(\mathbf{r},\mathbf{r};t)]_{\text{interference cross terms}} \longrightarrow \langle e^{-i(\theta-\theta')} \rangle e^{-i(\mathbf{k}-\mathbf{k}')\cdot\mathbf{r}}.$$
 (4.4.12)

This vanishes due to the random nature of θ and θ' . Thus one might conclude that atoms described by Eq. (4.4.11) would never yield spatial interference. This is not the case. If we use Eq. (4.4.11) to calculate $G^{(2)}(\mathbf{r}_1, \mathbf{r}_2; t, t)$, we find

$$G^{(2)}(\mathbf{r}_{1}, \mathbf{r}_{2}; t, t)$$

$$= |\alpha|^{2} \langle 1_{\mathbf{k}}, 1_{\mathbf{k}'} | E^{(-)}(\mathbf{r}_{1}) E^{(-)}(\mathbf{r}_{2}) E^{(+)}(\mathbf{r}_{2}) E^{(+)}(\mathbf{r}_{1}) | 1_{\mathbf{k}}, 1_{\mathbf{k}'} \rangle$$

$$= 2|\alpha|^{2} \mathscr{E}_{\mathbf{k}}^{4} \{ 1 + \cos[(\mathbf{k} - \mathbf{k}') \cdot (\mathbf{r}_{1} - \mathbf{r}_{2})] \}. \tag{4.4.13}$$

Here we see again that the random phases which destroy first-order coherence do not affect second-order HB-T type coherences.

THE HANBURY-BROWN-TWISS EFFECT FOR THERMAL AND LASER LIGHT

We now turn to the case of many-photon states associated with thermal and laser light and calculate the HB-T correlations for two such sources at S and S'.

As before, we look for the rate of coincidences in the photocount rates of detectors at \mathbf{r}_1 and \mathbf{r}_2 governed by the second-order correlation function

$$G^{(2)}(\mathbf{r}_1, \mathbf{r}_2; t, t) = \langle E^{(-)}(\mathbf{r}_1, t)E^{(-)}(\mathbf{r}_2, t)E^{(+)}(\mathbf{r}_2, t)E^{(+)}(\mathbf{r}_1, t)\rangle,$$
(4.4.14)

and consider the case in which the essential terms in the electric field operators $E(\mathbf{r}_i, t)$ (i = 1, 2) are given by

$$E^{(+)}(\mathbf{r}_i,t) = \mathscr{E}_{\mathbf{k}} \left(a_{\mathbf{k}} e^{-i\nu t + i\mathbf{k}\cdot\mathbf{r}_i} + a_{\mathbf{k}'} e^{-i\nu t + i\mathbf{k}'\cdot\mathbf{r}_i} \right), \tag{4.4.15}$$

where \mathbf{k} and \mathbf{k}' are the wave vectors of light from the two sources S and S'. Furthermore, as before, we are considering only equal frequency intervals such that $v = c|\mathbf{k}'| = c|\mathbf{k}'|$. Noting that only 'pairwise' operator orderings remain for thermal light, phase-diffused laser light, and light from two atoms (see Appendix 4.B), we have

$$G^{(2)}(\mathbf{r}_{1}, \mathbf{r}_{2}; t, t)$$

$$= \mathscr{E}_{\mathbf{k}}^{4} \left\langle \left(a_{\mathbf{k}}^{\dagger} e^{-i\mathbf{k}\cdot\mathbf{r}_{1}} + a_{\mathbf{k}'}^{\dagger} e^{-i\mathbf{k}'\cdot\mathbf{r}_{1}} \right) \left(a_{\mathbf{k}}^{\dagger} e^{-i\mathbf{k}\cdot\mathbf{r}_{2}} + a_{\mathbf{k}'}^{\dagger} e^{-i\mathbf{k}'\cdot\mathbf{r}_{2}} \right) \right.$$

$$\times \left(a_{\mathbf{k}} e^{i\mathbf{k}\cdot\mathbf{r}_{2}} + a_{\mathbf{k}'} e^{i\mathbf{k}'\cdot\mathbf{r}_{2}} \right) \left(a_{\mathbf{k}} e^{i\mathbf{k}\cdot\mathbf{r}_{1}} + a_{\mathbf{k}'} e^{i\mathbf{k}'\cdot\mathbf{r}_{1}} \right) \right\rangle$$

$$= \mathscr{E}_{\mathbf{k}}^{4} \left\langle a_{\mathbf{k}}^{\dagger} a_{\mathbf{k}}^{\dagger} a_{\mathbf{k}} a_{\mathbf{k}} + a_{\mathbf{k}'}^{\dagger} a_{\mathbf{k}'}^{\dagger} a_{\mathbf{k}'} a_{\mathbf{k}'} \right.$$

$$\left. + a_{\mathbf{k}}^{\dagger} a_{\mathbf{k}'}^{\dagger} a_{\mathbf{k}} a_{\mathbf{k}'} \left[1 + e^{-i(\mathbf{k} - \mathbf{k}')\cdot(\mathbf{r}_{1} - \mathbf{r}_{2})} \right] \right.$$

$$\left. + a_{\mathbf{k}'}^{\dagger} a_{\mathbf{k}}^{\dagger} a_{\mathbf{k}'} a_{\mathbf{k}} \left[1 + e^{i(\mathbf{k} - \mathbf{k}')\cdot(\mathbf{r}_{1} - \mathbf{r}_{2})} \right] \right\rangle. \tag{4.4.16}$$

If we assume $\langle n_{\mathbf{k}} \rangle = \langle n_{\mathbf{k}'} \rangle \equiv \langle n \rangle$ and likewise $\langle n_{\mathbf{k}}^2 \rangle = \langle n_{\mathbf{k}'}^2 \rangle \equiv \langle n^2 \rangle$, we may write Eq. (4.4.16) as

$$G^{(2)}(\mathbf{r}_{1}, \mathbf{r}_{2}; t, t)$$

$$= 2\mathscr{E}_{\mathbf{k}}^{4} \left(\langle n^{2} \rangle - \langle n \rangle + \langle n \rangle^{2} \left\{ 1 + \cos \left[(\mathbf{k} - \mathbf{k}') \cdot (\mathbf{r}_{1} - \mathbf{r}_{2}) \right] \right\} \right). (4.4.17)$$

Next we calculate $\langle n^2 \rangle$ for the two different cases in question: stars and phase-diffused laser light.

(a) Stars: the light from stars is thermal, therefore

$$\langle n^2 \rangle = 2 \langle n \rangle^2 + \langle n \rangle, \qquad \langle n \rangle = [\exp(\hbar v / k_{\rm B} T) - 1]^{-1},$$

and Eq. (4.4.17) yields

$$G^{(2)}(\mathbf{r}_{1}, \mathbf{r}_{2}; t, t) = 2\mathscr{E}_{\mathbf{k}}^{4} \left(2\langle n \rangle^{2} + \langle n \rangle^{2} \left\{ 1 + \cos \left[(\mathbf{k} - \mathbf{k}') \cdot (\mathbf{r}_{1} - \mathbf{r}_{2}) \right] \right\} \right).$$

$$(4.4.18)$$

The last term in Eq. (4.4.18) is the Hanbury-Brown-Twiss term which allows us to measure the angle between \mathbf{k} and \mathbf{k}' as in the discussion following Eq. (4.1.24).

(b) Lasers: far above threshold, the photon statistics for the lasers are Poissonian, therefore, $\langle n^2 \rangle = \langle n \rangle^2 + \langle n \rangle$, and we have

$$G^{(2)}(\mathbf{r}_{1}, \mathbf{r}_{2}; t, t) = 2\mathscr{E}_{\mathbf{k}}^{4} \Big(\langle n \rangle^{2} + \langle n \rangle^{2} \Big\{ 1 + \cos \left[(\mathbf{k} - \mathbf{k}') \cdot (\mathbf{r}_{1} - \mathbf{r}_{2}) \right] \Big\} \Big).$$

$$(4.4.19)$$

So, in both cases, we can measure the angular separation without the troublesome $\cos [(\mathbf{k} + \mathbf{k}') \cdot (\mathbf{r}_1 - \mathbf{r}_2)/2]$ -type terms which plague the Michelson stellar interferometer.

THE HANBURY-BROWN-TWISS SPATIAL INTERFERENCE EFFECT FOR NEUTRONS

By now, it is clear (contrary to what one frequently hears and reads) that the HB-T interference pattern, i.e., the interference cross terms in $G^{(2)}(\mathbf{r}_1, \mathbf{r}_2)$, has nothing to do with the boson nature of the photons. That is, the HB-T interference cross terms are present for radiation emitted by two independent atoms or lasers as shown in the previous two sections. In both of these cases, 'boson clumping' is absent.

Furthermore, it is clear from Eq. (4.4.4) and Fig. 4.9 that the effect carries over for neutrons as well. In such a case, the photon annihilation operators such as that given by Eq. (4.4.5) are replaced by a fermion operator of the form

$$\hat{\psi}(\mathbf{r}_{i},t) = c_{\mathbf{k}}e^{-i\nu t + i\mathbf{k}\cdot\mathbf{r}_{i}} + c_{\mathbf{k}'}e^{-i\nu t + i\mathbf{k}'\cdot\mathbf{r}_{i}}, \tag{4.4.20}$$

where the relevant fermion annihilation operators c_k and $c_{k'}$ now obey the anticommutation relations

$$c_{\mathbf{k}}c_{\mathbf{k}'}^{\dagger} + c_{\mathbf{k}'}^{\dagger}c_{\mathbf{k}} = \delta_{\mathbf{k},\mathbf{k}'},\tag{4.4.21}$$

$$c_{\mathbf{k}}^{\dagger} c_{\mathbf{k}'}^{\dagger} + c_{\mathbf{k}'}^{\dagger} c_{\mathbf{k}}^{\dagger} = 0, \tag{4.4.22}$$

$$c_{\mathbf{k}}c_{\mathbf{k}'} + c_{\mathbf{k}'}c_{\mathbf{k}} = 0. \tag{4.4.23}$$

Now Eq. (4.4.4) is replaced by the two-fermion wave function

$$\Psi^{(2)}(\mathbf{r}_{1}, t; \mathbf{r}_{2}, t) = \langle 0 | \hat{\psi}(\mathbf{r}_{2}, t) \hat{\psi}(\mathbf{r}_{1}, t) | \psi \rangle
= e^{-2i\nu t} \langle 0 | c_{\mathbf{k}} e^{i\mathbf{k}\cdot\mathbf{r}_{2}} c_{\mathbf{k}'} e^{i\mathbf{k}'\cdot\mathbf{r}_{1}} | 1_{\mathbf{k}}, 1_{\mathbf{k}'} \rangle
+ e^{-2i\nu t} \langle 0 | c_{\mathbf{k}'} e^{i\mathbf{k}'\cdot\mathbf{r}_{2}} c_{\mathbf{k}} e^{i\mathbf{k}\cdot\mathbf{r}_{1}} | 1_{\mathbf{k}}, 1_{\mathbf{k}'} \rangle,$$
(4.4.24)

and because

$$\langle 0|c_{\mathbf{k}}c_{\mathbf{k}'}|1_{\mathbf{k}}, 1_{\mathbf{k}'}\rangle = \langle 0|c_{\mathbf{k}}c_{\mathbf{k}'}c_{\mathbf{k}}^{\dagger}c_{\mathbf{k}'}^{\dagger}|0\rangle$$

$$= -\langle 0|c_{\mathbf{k}}c_{\mathbf{k}}^{\dagger}|0\rangle\langle 0|c_{\mathbf{k}'}c_{\mathbf{k}'}^{\dagger}|0\rangle$$

$$= -1, \qquad (4.4.25)$$

while an equivalent operator algebra for the second term in (4.4.24) yields +1, the fermion-fermion correlation function takes the form

$$G^{(2)}(\mathbf{r_1}, \mathbf{r_2}; t, t) = 2 \left\{ 1 - \cos[(\mathbf{k} - \mathbf{k}') \cdot (\mathbf{r_1} - \mathbf{r_2})] \right\}. \tag{4.4.26}$$

Thus we see that the Hanbury-Brown-Twiss effect works as well for two radiative point sources, S and S' of Fig. 4.9, emitting neutrons or β particles, as it does for γ rays or α particles. The only difference is the sign of the interference term.

4.4.2 Detection and measurement of squeezed states via homodyne detection

As seen earlier, direct photon count experiments, in which light of photon number distribution p(n) falls directly on a photodetector, provide information about the mean photon number and higher-order moments only. Such intensity measurements, therefore, are not particularly sensitive to squeezing but to antibunching and sub- or super-Poissonian statistics, which can also occur for nonsqueezed fields. Detection of squeezed states, on the other hand, requires a phase-sensitive scheme that measures the variance of a quadrature of the field. In this section, we consider the problem of detection of squeezed states of radiation via homodyne detection.

The schematic arrangement for homodyne detection is shown in

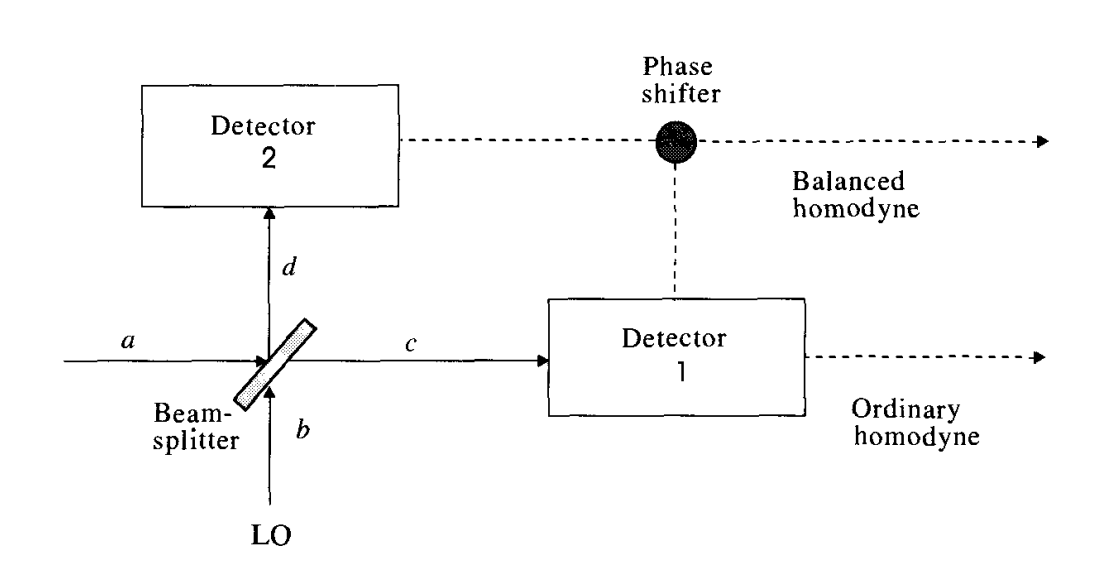


Fig. 4.10 Schematic diagram for homodyne detection.

Fig. 4.10. The input field is superimposed on the field from a local oscillator (LO) at a lossless beam-splitter of transmissivity T and reflectivity R such that R+T=1. The input and the oscillator modes are described by the annihilation operators a and b, respectively. Then denoting the two out-modes reaching photodetectors 1 and 2 by c and d, respectively, we have

$$c = \sqrt{T} a + i\sqrt{1 - T} b,$$
 (4.4.27)

$$d = i\sqrt{1-T} \ a + \sqrt{T} \ b. \tag{4.4.28}$$

There is a $\pi/2$ phase shift between the reflected and the transmitted waves for a symmetric beam-splitter which we have included by the factor *i* in Eqs. (4.4.27) and (4.4.28). The signals measured by the two detectors are determined by the operators

$$c^{\dagger}c = Ta^{\dagger}a + (1-T)b^{\dagger}b + i\sqrt{T(1-T)}(a^{\dagger}b - b^{\dagger}a), \quad (4.4.29)$$

$$d^{\dagger}d = (1 - T)a^{\dagger}a + Tb^{\dagger}b - i\sqrt{T(1 - T)}(a^{\dagger}b - b^{\dagger}a). \quad (4.4.30)$$

The frequency of the LO is equal to the input frequency so that the above operators do not have any time dependence. In the following we discuss the ordinary and balanced homodyne detectors.

Ordinary homodyne detection

In ordinary homodyne detection, the transmissivity of the beamsplitter is close to unity, i.e.,

$$T \gg R,\tag{4.4.31}$$

and only the photocurrent from detector 1 is measured. The LO mode is excited into a large amplitude coherent state $|\beta_l\rangle$ with phase ϕ_l . From Eq. (4.4.29) the signal reaching detector 1 is obtained as

$$\langle c^{\dagger}c\rangle = T\langle a^{\dagger}a\rangle + (1-T)|\beta_l|^2 - 2\sqrt{T(1-T)}|\beta_l|\langle X(\phi_l + \pi/2)\rangle,$$
(4.4.32)

where

$$X(\phi) \equiv X_{\phi} = \frac{1}{2}(ae^{-i\phi} + a^{\dagger}e^{i\phi}).$$
 (4.4.33)

We see that the signal contains the transmitted part of the input photons, reflected LO field, and most importantly, an interference term between the input field and the LO field. It is precisely this interference term that contains a quadrature of the input field depending upon the phase of the LO. In this detection scheme, a strong LO is used so that

$$(1-T)|\beta_l|^2 \gg T\langle a^{\dagger}a\rangle. \tag{4.4.34}$$

The inequalities (4.4.31) and (4.4.34) together imply that almost all the input field reaches the photodetector but the fraction of the LO field reaching the detector is still dominant. We can, therefore, neglect the first term in Eq. (4.4.32) and the mean number of photons in mode c is

$$\langle n_c \rangle = (1 - T)|\beta_l|^2 - 2\sqrt{T(1 - T)}|\beta_l|\langle X(\phi_l + \pi/2) \rangle.$$
 (4.4.35)

The first term constitutes a known constant value which can be subtracted from the signal and the remaining signal contains the quadrature of the input only.

The input and the LO modes are independent, i.e., $\langle ab \rangle = \langle a \rangle \langle b \rangle$. The photon number fluctuations can then be calculated in a straightforward manner using Eqs. (4.4.29) and (4.4.30)

$$(\Delta n_c)^2 = (1 - T)|\beta_l|^2 \{ (1 - T) + 4T [\Delta X(\phi_l + \pi/2)]^2 \}.$$
 (4.4.36)

In obtaining Eq. (4.4.36), we have used the inequality (4.4.34) and retained terms of second order in $|\beta_l|$. The signal noise is now seen to contain reflected LO noise (first term) and the transmitted input quadrature noise (second term). When the input is incoherent (or vacuum), $[\Delta X(\phi_l + \pi/2)]^2 = 1/4$, and the remaining term represents the LO shot noise. The squeezing condition for the input is

$$[\Delta X(\phi_l + \pi/2)]^2 < 1/4 \tag{4.4.37}$$

for certain values of the LO phase ϕ_l for which either quadrature X_1 or X_2 is squeezed.

In practice, the input is first blocked to determine the shot-noise level. The input is then allowed to reach the beam-splitter and the variance is determined with reference to the shot-noise level. Squeezing therefore manifests itself in sub-Poissonian statistics in homodyne detection.

Note, however, that intensity measurements in homodyne detection are quite different from those in direct detection, i.e., (a) intensity fluctuations in this case directly measure the fluctuations in a quadrature of the input, and (b) the signal and its variance depend upon the local oscillator phase angle, which is an external parameter.

BALANCED HOMODYNE DETECTION

In the discussion following Eq. (4.4.35), we assumed a perfectly coherent LO field and the oscillator excess noise has been neglected. The LO shot noise and the excess noise that enter through the reflectivity of the beam-splitter cannot be suppressed in ordinary homodyne detection because T, in principle, can never be 1. The LO noise can therefore limit ordinary homodyne detection. In particular, the detection is not quantum limited if the transmitted input noise is smaller than the reflected oscillator noise, as may be the case when the input noise is too small.

An alternative scheme is based on two-port homodyne detection which balances the output from the two ports of the beam-splitter. The fact that the noninterference terms at the two ports have the same sign and the interference terms appear with opposite signs (see Eqs. (4.4.29) and (4.4.30)) can be exploited to completely eliminate the noninterference terms. In this scheme, a 50/50 beam-splitter is used and the difference of two photodetector measurements is obtained. The output signal is determined by the operator

$$n_{cd} = c^{\dagger}c - d^{\dagger}d = -i(a^{\dagger}b - b^{\dagger}a).$$
 (4.4.38)

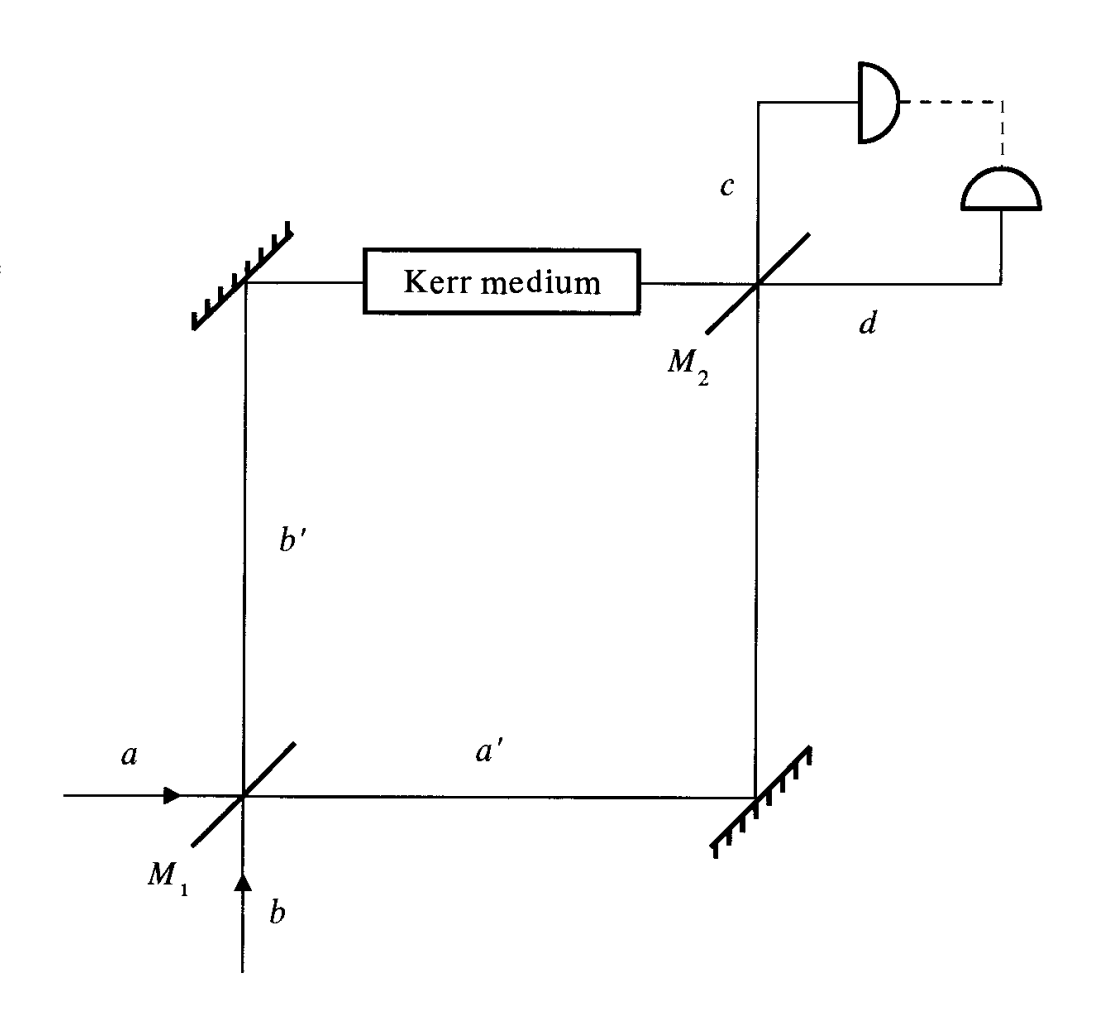
The measured signal then is

$$\langle n_{cd} \rangle = -2|\beta_l|\langle X(\phi_l + \pi/2) \rangle. \tag{4.4.39}$$

We see that the LO contribution to the signal has been eliminated and only the interference between the LO mean field and the input quadrature survives. The variance of the output signal can be found to be

$$(\Delta n_{cd})^2 = 4|\beta_l|^2 [\Delta X(\phi_l + \pi/2)]^2. \tag{4.4.40}$$

Fig. 4.11
A Mach-Zehnder interferometer with a phase sensitive element in the upper arm operating in the balanced mode. The operators a and b are the annihilation operators for the signal and local oscillator modes.



Here once again we assume a strong LO. The dominant term now is only due to the interference between the input signal noise and the LO power, and the LO noise is eliminated completely. This makes the strong LO condition less stringent in this case.

MEASUREMENT OF PHASE UNCERTAINTY*

The use of balanced homodyne detection in precision interferometry yields several interesting results. Here we discuss the application of balanced homodyne detection in the measurement of phase uncertainty of optical signals.

The system is depicted in Fig. 4.11, where we see a Mach–Zehnder interferometer with a phase sensitive element in the upper arm operating in the balanced mode. The phase sensitive element introduces a phase shift ϕ_p , e.g., by a Kerr effect medium discussed in Section 19.2.

We assume M_1 and M_2 in Fig. 4.11 to be 50/50 beam-splitters

^{*} This section follows, in part, the unpublished lecture notes of B. Yurke, to whom the authors are indebted.

and assume the two path lengths between them to be equal. The annihilation operators of the various modes in Fig. 4.11 are related to each other via

$$a' = \frac{1}{\sqrt{2}}(a+ib),\tag{4.4.41}$$

$$b' = \frac{1}{\sqrt{2}}(ia + b),\tag{4.4.42}$$

and

$$c = \frac{1}{\sqrt{2}} \left(a' + ib'e^{i\phi_p} \right)$$

$$= \frac{1}{2} \left[\left(1 - e^{i\phi_p} \right) a + i \left(1 + e^{i\phi_p} \right) b \right],$$

$$d = \frac{1}{\sqrt{2}} \left(ia' + b'e^{i\phi_p} \right)$$

$$= \frac{1}{2} \left[i \left(1 + e^{i\phi_p} \right) a - \left(1 - e^{i\phi_p} \right) b \right].$$
(4.4.44)

(4.4.44)

Here, as before, we assume a $\pi/2$ phase shift for the reflected field.

The output signal in the balanced homodyne detector is given by the operator

$$n_{cd} = c^{\dagger}c - d^{\dagger}d$$

$$= (b^{\dagger}b - a^{\dagger}a)\cos\phi_p - (a^{\dagger}b + b^{\dagger}a)\sin\phi_p. \tag{4.4.45}$$

If the local oscillator mode is in a large amplitude coherent state $|\beta_l\rangle$ and the signal mode is in a vacuum state $|0\rangle$, the signal is

$$\langle n_{cd} \rangle = n_l \cos \phi_p, \tag{4.4.46}$$

where $n_l = |\beta_l|^2$.

It is interesting to note that, for $\phi_p = \pi/2$,

$$n_{cd} = -(a^{\dagger}b + b^{\dagger}a),$$
 (4.4.47)

i.e., n_{cd} does not depend on the photon number operators and the system in Fig. 4.11 is essentially equivalent to a balanced homodyne detector of Fig. 4.10.

Now, for the signal mode in a vacuum state, the difference operator (4.4.47) has a variance

$$(\Delta n_{cd})^2 = |\beta_l|^2 = n_l. \tag{4.4.48}$$

This can be related to the phase error by noting that, from Eq. (4.4.46), we have

$$\frac{\partial \langle n_{cd} \rangle}{\partial \phi_p} = -n_l \sin \phi_p, \tag{4.4.49}$$

and, since on balance $(\phi_p = \pi/2)$,

$$\left|\frac{\partial \langle n_{cd} \rangle}{\partial \phi_p}\right| = n_l. \tag{4.4.50}$$

Hence the phase error is given by

$$\Delta \phi = \frac{\Delta n_{cd}}{|\partial \langle n_{cd} \rangle / \partial \phi_p|} = \frac{\sqrt{n_l}}{n_l}$$

$$= \frac{1}{\sqrt{n_l}}.$$
(4.4.51)

If we now take the signal to be a squeezed vacuum state, $|0, \xi\rangle$ with $\xi = r \exp(i\theta)$,

$$\langle n_{cd} \rangle = (n_l + \sinh^2 r) \cos \phi_p$$

 $\cong n_l \cos \phi_p.$ (4.4.52)

On balance, $\phi_p = \pi/2$, $|\partial \langle n_{cd} \rangle / \partial \phi_p| = n_l$, and

$$(\Delta n_{cd})^2 = n_l[\cosh 2r - \cos(\theta - 2\phi_l)\sinh 2r] + \sinh^2 r, \quad (4.4.53)$$

where we have used Eqs. (2.7.11)–(2.7.13). If we take $\theta=2\phi_l$, Eq. (4.4.53) becomes

$$(\Delta n_{cd})^2 = n_l e^{-2r} + \sinh^2 r, \tag{4.4.54}$$

and, for $n_l \gg 1$, we may neglect the $\sinh^2 r$ term in Eq. (4.4.54) to yield the reduced phase noise

$$\Delta \phi = \frac{\Delta n_{cd}}{|\partial \langle n_{cd} \rangle / \partial \phi_p|}$$

$$= \frac{e^{-r}}{\sqrt{n_l}}.$$
(4.4.55)

4.4.3 Interference of two photons

We now describe an experiment in which the joint probability for the detection of two photons at two points is measured as a function of the separation between the points. This two-photon interference experiment is an example of the intensity correlation experiment where the predictions of the quantum theoretical analysis are quite different from the corresponding predictions of the classical coherence theory. The experimental results agree with the predictions of the quantum coherence theory for the choice of parameters where the classical and quantum theories yield different results. The existence of nonclassical effects in two-photon interference is just one example of a large number of related phenomena where the quantum nature of light is exhibited

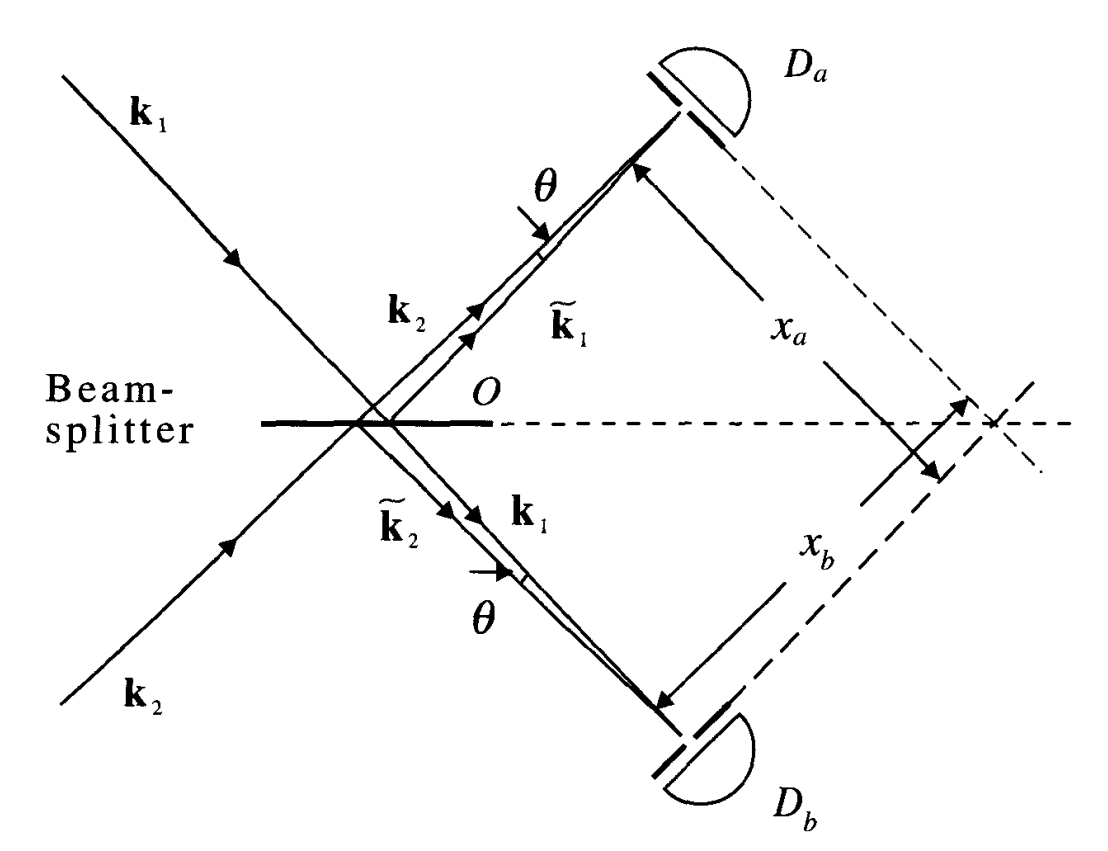


Fig. 4.12 Schematic diagram for the two-photon interference experiment. (From Z. Y. Ou and L. Mandel, *Phys. Rev.* Lett. **62**, 2941 (1989).)

explicitly. Some of these phenomena will be discussed later in this book, particularly in Chapter 21.

In the two-photon interferometer, two randomly phased light waves of narrow bandwidth impinge simultaneously on the surface of a beam-splitter. The reflected and transmitted waves are brought together on the detectors D_a and D_b located at \mathbf{r}_a and \mathbf{r}_b , respectively, as shown in Fig. 4.12. The outputs, after amplification, are sent to a correlator. The measured coincidence rate provides a measure of the joint detection probability $P(x_a, x_b)\delta x_a\delta x_b$ of detection at x_a and x_b within δx_a and δx_b , respectively. Here x_a and x_b are the projections of \mathbf{r}_a and \mathbf{r}_b onto the vectors $\mathbf{k}_2 - \mathbf{k}_1$ and $\mathbf{k}_2 - \mathbf{k}_1$, respectively (see Fig. 4.12), where \mathbf{k}_1 , \mathbf{k}_2 are the wave vectors corresponding to \mathbf{k}_1 , \mathbf{k}_2 after reflection at the beam-splitter.

As discussed in Section 4.2, the joint detection probability is governed by w_2 . We thus have

$$P(x_a, x_b) = \kappa_a \kappa_b \langle E^{(-)}(x_a) E^{(-)}(x_b) E^{(+)}(x_b) E^{(+)}(x_a) \rangle, \quad (4.4.56)$$

where κ_a and κ_b are factors which depend on the characteristics of the detectors. We now calculate the joint detection probability for incident correlated photons within the framework of both quantum and classical coherence theories.

If we treat O (see Fig. 4.12) as the origin, we can express the positive frequency part of the fields $E^{(+)}(x_a)$ and $E^{(+)}(x_b)$ in the form

$$E^{(+)}(x_a) = \mathscr{E}\left(i\sqrt{R}a_1e^{i\tilde{\mathbf{k}}_1\cdot\mathbf{r}_a} + \sqrt{T}a_2e^{i\mathbf{k}_2\cdot\mathbf{r}_a}\right),\tag{4.4.57}$$

$$E^{(+)}(x_b) = \mathscr{E}\left(\sqrt{T}a_1e^{i\mathbf{k}_1\cdot\mathbf{r}_b} + i\sqrt{R}a_2e^{i\tilde{\mathbf{k}}_2\cdot\mathbf{r}_b}\right),\tag{4.4.58}$$

where R and T are the reflectivity and the transmittivity of the beam-splitter, a_1 and a_2 are the destruction operators for the input fields at the beam-splitter, and $\mathscr{E} = (\hbar v/2\epsilon_0 V)^{1/2}$. If the beam-splitter is 50/50, then R = T = 1/2. Equations (4.4.57) and (4.4.58) then simplify and are given in the form

$$E^{(+)}(x_a) = \frac{\mathscr{E}}{\sqrt{2}}(ia_1e^{i\mathbf{k}_1\cdot\mathbf{r}_a} + a_2e^{i\mathbf{k}_2\cdot\mathbf{r}_a}), \tag{4.4.59}$$

$$E^{(+)}(x_b) = \frac{\mathscr{E}}{\sqrt{2}} (a_1 e^{i\mathbf{k}_1 \cdot \mathbf{r}_b} + ia_2 e^{i\tilde{\mathbf{k}}_2 \cdot \mathbf{r}_b}). \tag{4.4.60}$$

The initial state of the field for single photons is the two-photon Fock state $|1_1, 1_2\rangle$. Such a state can be prepared in the process of degenerate parametric amplification in a nonlinear medium (Chapter 16). The joint detection probability density, Eq. (4.4.56), is therefore given by

$$P(x_{a}, x_{b}) = \kappa_{a} \kappa_{b} \langle 1_{1}, 1_{2} | E^{(-)}(x_{a}) E^{(-)}(x_{b}) E^{(+)}(x_{b}) E^{(+)}(x_{a}) | 1_{1}, 1_{2} \rangle$$

$$= \frac{1}{2} \kappa_{a} \kappa_{b} \mathscr{E}^{4}$$

$$\{1 - \cos[(\mathbf{k}_{2} - \tilde{\mathbf{k}}_{1}) \cdot \mathbf{r}_{a} - (\tilde{\mathbf{k}}_{2} - \mathbf{k}_{1}) \cdot \mathbf{r}_{b}]\} \qquad (4.4.61)$$

where we have substituted for $E^{(+)}(x_a)$ and $E^{(+)}(x_b)$ and their Hermitian conjugates from Eqs. (4.4.59) and (4.4.60). If the angles θ between $\tilde{\mathbf{k}}_1$ and \mathbf{k}_2 and between $\tilde{\mathbf{k}}_2$ and \mathbf{k}_1 are very small, then the associated interference pattern has a fringe spacing given by

$$L \approx \frac{2\pi}{|\tilde{\mathbf{k}}_1 - \mathbf{k}_2|} = \frac{2\pi}{|\tilde{\mathbf{k}}_2 - \mathbf{k}_1|} \approx \frac{2\pi}{k\theta},\tag{4.4.62}$$

where $k = |\mathbf{k}_1| = |\mathbf{k}_2|$, and we obtain

$$P(x_a, x_b) = \frac{1}{2} \kappa_a \kappa_b \mathscr{E}^4 \{ 1 - \cos[2\pi (x_a - x_b)/L] \}.$$
 (4.4.63)

Thus the joint detection probability exhibits a cosine modulation in $x_a - x_b$ with visibility

$$U = \frac{P_{\text{max}} - P_{\text{min}}}{P_{\text{max}} + P_{\text{min}}} = 1. \tag{4.4.64}$$

Therefore, there is an interference between two two-photon amplitudes associated with both photons being reflected and both photons being transmitted.

A unity visibility implies that if a photon is detected at the position x_a then there are certain positions x_b where the other photon cannot be found, and vice versa. This situation is in contrast to classical optics (as seen below) which predicts a nonvanishing optical field at both positions x_a and x_b .

Next we calculate the visibility by treating the incident fields classically. We can replace the operators a_1 and a_2 in Eqs. (4.4.59) and (4.4.60) by the classical c-number amplitudes α_1 and α_2 , respectively. We also assume that the fields have random phases. This is a reasonable assumption because the single-photon states have arbitrary phase. The classical ensemble averages of phase-dependent quantities, such as α_1 and $|\alpha_1|^2\alpha_2$, therefore vanish.

The joint detection probability $P(x_a, x_b)$ is now given by Eq. (4.4.56) where $E^{(+)}$ and $E^{(-)}$ are classical c-number fields and the angle brackets indicate the classical ensemble average. It is readily seen that

$$P(x_a, x_b) = \frac{1}{4} \kappa_a \kappa_b \{ \langle (I_1 + I_2)^2 \rangle - 2 \langle I_1 I_2 \rangle \cos[2\pi (x_a - x_b)/2] \},$$
(4.4.65)

where $I_1 = \mathscr{E}^2 |\alpha_1|^2$ and $I_2 = \mathscr{E}^2 |\alpha_2|^2$. The visibility U of the interference is given by

$$U = \frac{2\langle I_1 I_2 \rangle}{\langle I_1^2 \rangle + \langle I_2^2 \rangle + 2\langle I_1 I_2 \rangle}.$$
 (4.4.66)

As $\langle I_1^2 \rangle + \langle I_2^2 \rangle \ge 2 \langle I_1 I_2 \rangle$, it follows that

$$U \le \frac{1}{2},\tag{4.4.67}$$

which gives a classical limit. This shows that the visibility cannot exceed 50 percent in contradiction to the prediction of the quantum mechanical result.

An observation of a larger than 50 percent visibility therefore corresponds to nonclassical behavior. A visibility of over 75 percent has been observed in the two-photon interference experiments.

4.4.4 Photon antibunching, Poissonian, and sub-Poissonian light

In Section 4.2 we showed that a correspondence between the quantum and classical coherence theories can be established via *P*-representation.

However, as we discussed, the *P*-representation does not have all the properties of a classical distribution function. Thus it is possible that certain inequalities for the correlation functions which implicitly assume a well-defined probability distribution may not be satisfied. A violation of these inequalities for certain radiation fields would therefore provide explicit evidence for the quantum nature of light. In this section we consider some examples of such fields.

In the classical coherence theory, the field operators are replaced by c-number fields. For such classical fields, it follows from the Schwarz inequality, $|\langle a^*b\rangle|^2 \le \langle |a|^2\rangle\langle |b|^2\rangle$ (with $a=I(\mathbf{r},t)$ and $b=I(\mathbf{r},t+\tau)$), that

$$|\langle I(\mathbf{r},t)I(\mathbf{r},t+\tau)\rangle|^2 \le \langle I^2(\mathbf{r},t)\rangle \langle I^2(\mathbf{r},t+\tau)\rangle. \tag{4.4.68}$$

The corresponding inequality in the quantum coherence theory is obtained by replacing the product of intensities within the angle brackets by the corresponding normally ordered operators, i.e.,

$$|\langle : I(\mathbf{r}, t)I(\mathbf{r}, t + \tau) : \rangle|^2 \le \langle : I^2(\mathbf{r}, t) : \rangle \langle : I^2(\mathbf{r}, t + \tau) : \rangle, \quad (4.4.69)$$

where : represents normal ordering, i.e., the creation operators to the left and the annihilation operators to the right. This inequality is satisfied for fields with a well-defined P-representation. It follows from the definition of $g^{(2)}(\tau)$ (Eq. (4.2.21)), that, for statistically stationary fields, this inequality can be recast in the following simple form

$$g^{(2)}(\tau) \le g^{(2)}(0). \tag{4.4.70}$$

This inequality was seen to be satisfied by thermal and coherent light. We recall from the definition of $g^{(2)}(\tau)$ that it is a measure of the photon correlations between some time t and a later time $t + \tau$. When the field satisfies the inequality $g^{(2)}(\tau) < g^{(2)}(0)$ for $\tau < \tau_c$, the photons exhibit excess correlations for times less than the correlation time τ_c . This is called *photon bunching* as the photons tend to distribute themselves preferentially in bunches rather than at random. When such a light beam falls on a photodetector, more photon pairs are detected close together than further apart (Fig. 4.13(a)). The thermal field is an example of photon bunching.

In certain quantum optical systems, the inequality (4.4.70) may be violated with the result

$$g^{(2)}(\tau) > g^{(2)}(0).$$
 (4.4.71)

This would correspond to the phenomenon of *photon antibunching*. This is the opposite effect, in which fewer photon pairs are detected

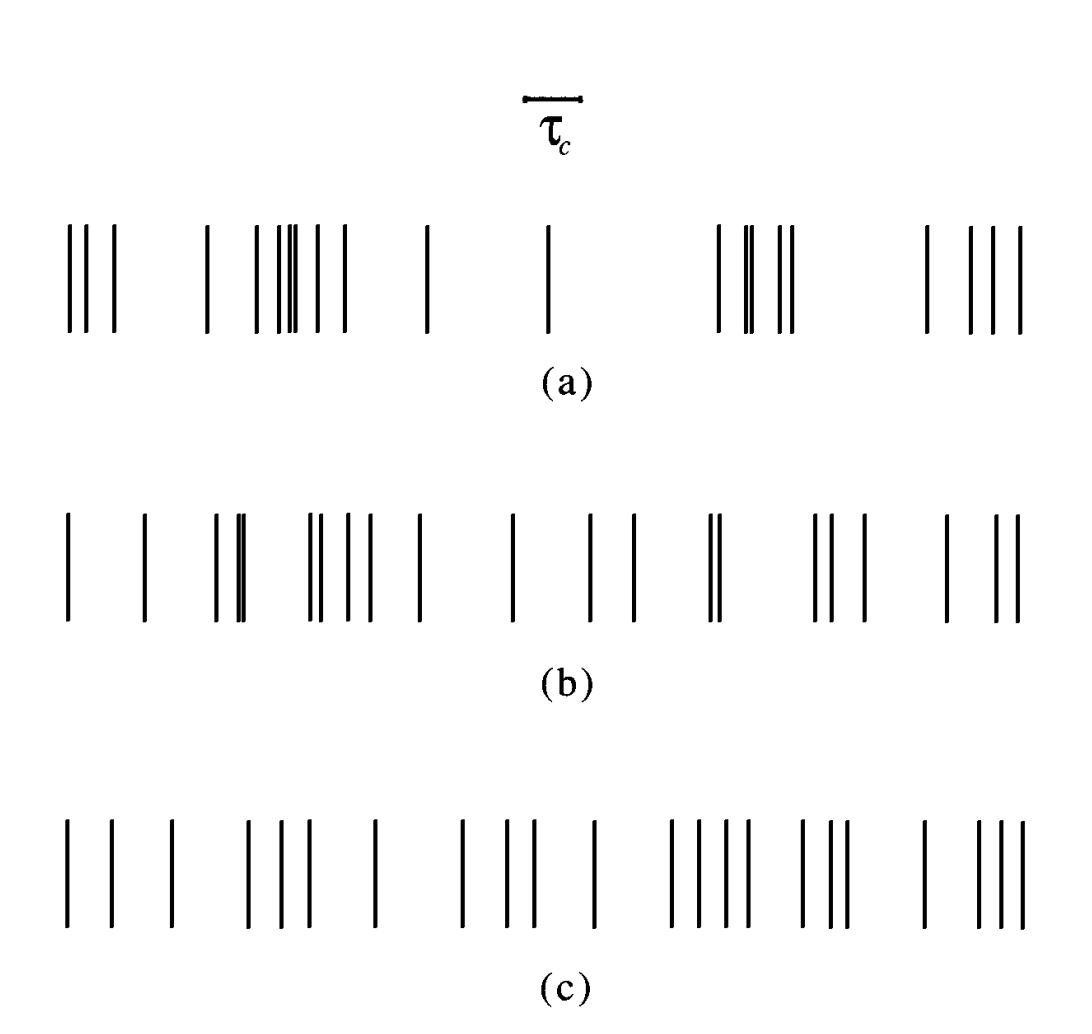


Fig. 4.13
Photon counts as functions of time for light beams which are (a) bunched, (b) random, and (c) antibunched.

close together than further apart (Fig. 4.13(c)). Photon antibunching will be discussed in the process of resonance fluorescence from an atom in Section 10.6.

Another nonclassical inequality is given by

$$g^{(2)}(0) < 1. (4.4.72)$$

This nonclassical inequality is satisfied by fields whose P-representation is not nonnegative definite. To see this explicitly, we first rewrite this inequality, after some rearrangement, in the form (see Eq. (4.2.21))

$$(\langle a^{\dagger} a^{\dagger} a a \rangle - \langle a^{\dagger} a \rangle^2) < 0, \tag{4.4.73}$$

or, in terms of the P-representation,

$$\int P(\alpha, \alpha^*)(|\alpha|^2 - \langle a^{\dagger} a \rangle)^2 d^2 \alpha < 0. \tag{4.4.74}$$

Since $(|\alpha|^2 - \langle a^{\dagger}a \rangle)^2$ is positive definite for all values of α , the only way this inequality may be satisfied is if $P(\alpha, \alpha^*)$ is negative for at

least some values of α . Thus $P(\alpha, \alpha^*)$ does not satisfy the properties of a classical distribution function. The inequality (4.4.72) is satisfied by fields whose photon distribution function is narrower than the Poisson distribution. Such fields are referred to as *sub-Poissonian*. Fields for which $g^{(2)}(0) = 1$ and $g^{(2)}(0) > 1$ are similarly referred to as *Poissonian* and *super-Poissonian*, respectively. For example, a thermal field for which $g^{(2)}(0) = 2$ is super-Poissonian, a field in a coherent state $|\alpha_0\rangle$ for which $g^{(2)}(0) = 1$ is Poissonian, and the field in a number state $|n_0\rangle$ for which $g^{(2)}(0) = 1 - 1/n_0$ is sub-Poissonian.

It is evident from the above discussion that many other field states can be constructed for which the P-representation will not be well-behaved. One such state is the squeezed state of the radiation field. To show this, we express $(\Delta X_i)^2$ (i=1,2) as an average with respect to the P-representation:

$$(\Delta X_i)^2 = \frac{1}{4} + (:\Delta X_i:)^2$$

$$= \frac{1}{4} \left\{ 1 + \int d^2 \alpha P(\alpha, \alpha^*) [(\alpha + \alpha^*) - (\langle \alpha \rangle + \langle \alpha^* \rangle)]^2 \right\}.$$
(4.4.75)

The condition for squeezing $(\Delta X_i)^2 < 1/4$ (i = 1 or 2) requires that $P(\alpha, \alpha^*)$ is negative for at least some values of α , i.e., it is not "nonnegative definite". A squeezed state of the radiation field, therefore, is a nonclassical state.

4.5 Photon counting and photon statistics

In this section we determine the photoelectron counting statistics produced by a fully quantum mechanical field. The problem of obtaining the photocount distribution from the photon statistics can be solved in a completely quantum mechanical fashion. Here we give a simple derivation of this relationship based on a simple probabilistic argument.

Let the probability of having a photoelectron ejected from a detector interacting with a field having just one photon $|1\rangle$ for a certain time be given by η . The quantum efficiency η depends on the characteristics of the detector atoms and the interaction time. Now, if the state of the radiation field is $|n\rangle$, the probability of observing m photoelectrons, $P_m^{(n)}$, is proportional to η^m which is to be multiplied by the probability that (n-m) quanta were not absorbed, i.e., $(1-\eta)^{n-m}$. This gives

$$P_m^{(n)} \propto \eta^m (1 - \eta)^{n - m}. \tag{4.5.1}$$

However, we do not know which m photons of the original number n were absorbed, so we must include a combinatorial factor:

$$P_m^{(n)} = \binom{n}{m} \eta^m (1 - \eta)^{n - m}. \tag{4.5.2}$$

This is Bernoulli's distribution for m successful events (counts) and n-m failures, each event having a probability η . Since we have a distribution of n values given by the photon distribution function ρ_{nn} , we must multiply Eq. (4.5.2) by ρ_{nn} and sum over n:

$$P_m = \sum_{n} P_m^{(n)} \rho_{nn}, \tag{4.5.3}$$

which yields the following expression for the photoelectron counting distribution:

$$P_{m} = \sum_{n=m}^{\infty} {n \choose m} \eta^{m} (1 - \eta)^{n-m} \rho_{nn}. \tag{4.5.4}$$

This expression is valid for all η ($0 \le \eta \le 1$). Clearly, if we wish to obtain the photon statistics by counting photoelectrons, we must require $\eta = 1$. In that case, we obtain from Eq. (4.5.4)

$$P_m = \rho_{mm}. \tag{4.5.5}$$

In all other cases, $\eta < 1$, and the measured photoelectron statistics can be very different from the photon statistics.

Alternatively, we can write P_m in terms of the P-representation, $P(\alpha, \alpha^*)$, of the field by noting that

$$\rho_{nn} = \int d^2 \alpha P(\alpha, \alpha^*) \frac{|\alpha|^{2n}}{n!} e^{-|\alpha|^2}, \qquad (4.5.6)$$

so that Eq. (4.5.4) becomes

$$P_{m} = \int d^{2}\alpha \sum_{n=m}^{\infty} {n \choose m} P(\alpha, \alpha^{*}) \frac{|\alpha|^{2n}}{n!} e^{-|\alpha|^{2}} \eta^{m} (1 - \eta)^{n-m}. \quad (4.5.7)$$

By changing n to $\ell + m$ and summing over ℓ , we obtain

$$P_m = \int d^2 \alpha P(\alpha, \alpha^*) \frac{(\eta |\alpha|^2)^m}{m!} e^{-\eta |\alpha|^2}. \tag{4.5.8}$$

It may be pointed out that this equation can be inverted, i.e., it is possible to derive the P-representation of the field from the knowledge of P_m , given that ρ is diagonal in the n representation.

Appendix 4.A 139

4.A Classical and quantum descriptions of two-source interference

Classically, the radiation from the two slits in Young's experiment is correctly described by two spherical waves. In the notation of Fig. 4.14, the intensity at the screen then goes as

$$I(\mathbf{r}) = \left| \frac{\mathscr{E}e^{ikr_1}}{r_1} + \frac{\mathscr{E}e^{ikr_2}}{r_2} \right|^2, \tag{4.A.1}$$

and the interference cross term is given by

$$I_{12} = \frac{\mathscr{E}^*\mathscr{E}}{r_1 r_2} e^{ik(r_1 - r_2)} + \text{c.c.}$$
 (4.A.2)

Noting that $r_{1,2} = \sqrt{D^2 + (x \mp d)^2} \cong D + d^2/(2D) \mp xd/D$, where the '-' goes with source 1 and the '+' with source 2, we have

$$I_{12} \cong \frac{\mathscr{E}^*\mathscr{E}}{r^2} e^{-2ikxd/D} + \text{c.c.}$$
 (4.A.3)

However, some texts give a plane-wave treatment of Young's setup, in which it is argued that the radiation at the detector site \mathbf{r} consists of two plane waves. In such a case, we have

$$I(\mathbf{r}) = \left| \mathscr{E}_0 e^{\mathbf{k}_1 \cdot \mathbf{r}} + \mathscr{E}_0 e^{\mathbf{k}_2 \cdot \mathbf{r}} \right|^2, \tag{4.A.4}$$

and the interference cross term is

$$I_{12}(\mathbf{r}) = \mathscr{E}_0^* \mathscr{E}_0 e^{i(\mathbf{k}_1 - \mathbf{k}_2) \cdot \mathbf{r}} + \text{c.c.}$$
 (4.A.5)

Hence if, in the notation of Fig. 4.14, we write $\mathbf{k}_i = k(\hat{z}\cos\theta_i + \hat{x}\sin\theta_i)$, then $\mathbf{k}_i \cdot \mathbf{r} = k(D\cos\theta_i + x\sin\theta_i) \cong k(D \mp xd/D)$, where the ' \mp ' signs go with 1 and 2, and we find

$$I_{12}(\mathbf{r}) \cong \mathscr{E}_0^* \mathscr{E}_0 e^{-2ikxd/D} + \text{c.c.}, \tag{4.A.6}$$

in agreement with the spherical-wave treatment.

The quantum field theoretic description of Young's experiment is well illustrated by replacing the two slits by two atoms as in Section 4.3.2 and Section 21.1. There the state vector for the photon emitted by the ith atom is given by

$$|\gamma_i\rangle = \sum_{\mathbf{k}} \frac{g_{\mathbf{k}} e^{-i\mathbf{k}\cdot\mathbf{d}_i}}{(\nu_{\mathbf{k}} - \omega) + i\Gamma/2} |1_{\mathbf{k}}\rangle,$$
 (4.A.7)

where g_k is a constant depending on the strength of atom-field coupling, ω is the atomic frequency between levels $|a\rangle$ and $|b\rangle$, Γ is the

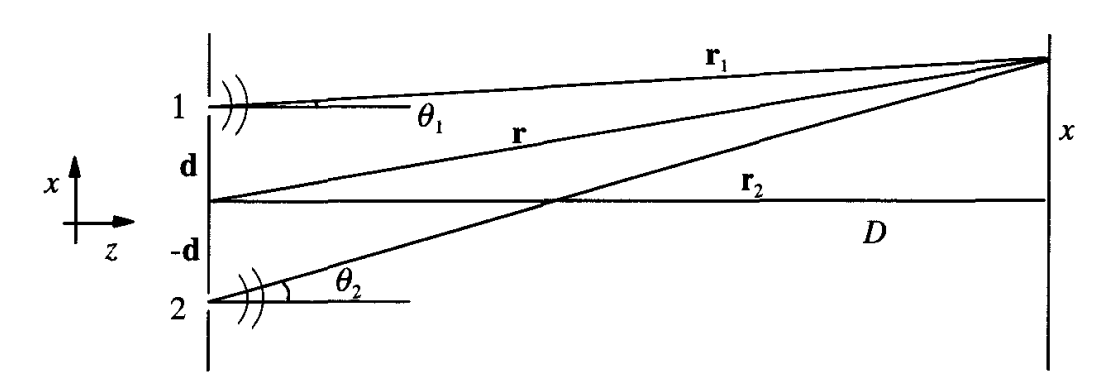


Fig. 4.14 Schematic diagram for a plane-wave treatment of Young's setup.

decay rate for the $|a\rangle \rightarrow |b\rangle$ transition, and \mathbf{d}_i is the position of the *i*th atom. The correlation function for the scattered field is then found to be

$$G^{(1)}(\mathbf{r}, \mathbf{r}; 0) = \frac{1}{2} \left| \langle 0 | E^{(+)}(\mathbf{r}, t) | \gamma_1 \rangle + \langle 0 | E^{(+)}(\mathbf{r}, t) | \gamma_2 \rangle \right|^2$$

$$= \left| \frac{\tilde{\mathscr{E}} e^{ikr_1}}{r_1} + \frac{\tilde{\mathscr{E}} e^{ikr_2}}{r_2} \right|^2, \qquad (4.A.8)$$

where $\tilde{\mathscr{E}}$ is an effective electric field. Thus we have the same result as in the classical spherical-wave problem.

Finally, we note that single photon plane-wave states can be used to demonstrate the two-source interference fringes. At the risk of belaboring the obvious, we note that if we consider the radiation from source 1 to be described by the single photon state $|1_{\mathbf{k}_1}\rangle$, and that from source 2 by $|1_{\mathbf{k}_2}\rangle$, then we have $|\psi\rangle = (|1_{\mathbf{k}_1}\rangle + |1_{\mathbf{k}_2}\rangle)/\sqrt{2}$ and

$$G^{(1)}(\mathbf{r}, \mathbf{r}; 0) = \langle \psi | E^{(-)}(\mathbf{r}, t) E^{(+)}(\mathbf{r}, t) | \psi \rangle$$

$$= \frac{1}{2} \left| \langle 0 | E^{(+)}(\mathbf{r}, t) | 1_{\mathbf{k}_{1}} \rangle + \langle 0 | E^{(+)}(\mathbf{r}, t) | 1_{\mathbf{k}_{2}} \rangle \right|^{2}$$

$$= \mathscr{E}_{0}^{*} \mathscr{E}_{0} \left| e^{i\mathbf{k}_{1} \cdot \mathbf{r}} + e^{i\mathbf{k}_{2} \cdot \mathbf{r}} \right|^{2}. \tag{4.A.9}$$

Here again, interference is observed as in the classical case, and the utilization of both states $|\gamma_i\rangle$ and $|1_{\mathbf{k}_i}\rangle$ in Young-type experiments is justified.

4.B Calculation of the second-order correlation function

From Eqs. (4.4.14) and (4.4.15), we have (note that some terms are underlined)

Problems 141

$$G^{(2)}(\mathbf{r}_{1},\mathbf{r}_{2};t,t)$$

$$= \mathcal{E}_{\mathbf{k}}^{4} \langle [a_{\mathbf{k}}^{\dagger}(1) + a_{\mathbf{k}'}^{\dagger}(1)] [a_{\mathbf{k}}^{\dagger}(2) + a_{\mathbf{k}'}^{\dagger}(2)] [a_{\mathbf{k}}(2) + a_{\mathbf{k}'}(2)]$$

$$= a_{\mathbf{k}}^{4} \langle a_{\mathbf{k}}^{\dagger}(1) a_{\mathbf{k}}^{\dagger}(2) a_{\mathbf{k}}(2) a_{\mathbf{k}}(1)$$

$$+ [a_{\mathbf{k}}^{\dagger}(1) a_{\mathbf{k}}^{\dagger}(2) a_{\mathbf{k}}(2) a_{\mathbf{k}'}(1) + a_{\mathbf{k}}^{\dagger}(1) a_{\mathbf{k}}^{\dagger}(2) a_{\mathbf{k}'}(2) a_{\mathbf{k}}(1)$$

$$+ a_{\mathbf{k}}^{\dagger}(1) a_{\mathbf{k}'}^{\dagger}(2) a_{\mathbf{k}}(2) a_{\mathbf{k}'}(1)]$$

$$+ a_{\mathbf{k}}^{\dagger}(1) a_{\mathbf{k}'}^{\dagger}(2) a_{\mathbf{k}}(2) a_{\mathbf{k}'}(1) + a_{\mathbf{k}}^{\dagger}(1) a_{\mathbf{k}'}^{\dagger}(2) a_{\mathbf{k}'}(2) a_{\mathbf{k}'}(1)$$

$$+ [a_{\mathbf{k}}^{\dagger}(1) a_{\mathbf{k}'}^{\dagger}(2) a_{\mathbf{k}}(2) a_{\mathbf{k}}(1) + a_{\mathbf{k}'}^{\dagger}(1) a_{\mathbf{k}'}^{\dagger}(2) a_{\mathbf{k}'}(2) a_{\mathbf{k}'}(1)]$$

$$+ a_{\mathbf{k}'}^{\dagger}(1) a_{\mathbf{k}}^{\dagger}(2) a_{\mathbf{k}}(2) a_{\mathbf{k}'}(1) + a_{\mathbf{k}'}^{\dagger}(1) a_{\mathbf{k}}^{\dagger}(2) a_{\mathbf{k}'}(2) a_{\mathbf{k}'}(1)]$$

$$+ [a_{\mathbf{k}'}^{\dagger}(1) a_{\mathbf{k}'}^{\dagger}(2) a_{\mathbf{k}'}(2) a_{\mathbf{k}'}(1)$$

$$+ [a_{\mathbf{k}'}^{\dagger}(1) a_{\mathbf{k}'}^{\dagger}(2) a_{\mathbf{k}'}(2) a_{\mathbf{k}'}(1)$$

$$+ [a_{\mathbf{k}'}^{\dagger}(1) a_{\mathbf{k}'}^{\dagger}(2) a_{\mathbf{k}}(2) a_{\mathbf{k}'}(1)]$$

$$+ (a_{\mathbf{k}'}^{\dagger}(1) a_{\mathbf{k}'}^{\dagger}(2) a_{\mathbf{k}}(2) a_{\mathbf{k}'}(1)$$

$$+ (a_{\mathbf{k}'}^{\dagger}(1) a_{\mathbf{k}'}^{\dagger}(2) a_{\mathbf{k}}(2) a_{\mathbf{k}'}(2)$$

$$+ (a_{\mathbf{k}'}^{\dagger}(1) a_{\mathbf{k}'}^{\dagger}(2) a_{\mathbf{k}}(2) a_{\mathbf{k}'}(2)$$

$$+ (a_{\mathbf{k}'}^{\dagger}(1) a_{\mathbf{k}'}^{\dagger}(2) a_{\mathbf{k}'}(2) a_{\mathbf{k}'}(2)$$

$$+ (a_{\mathbf{k}'}^{\dagger}(1) a_{\mathbf{k}'}$$

where

$$a_{\mathbf{k}}^{\dagger}(i) = a_{\mathbf{k}}^{\dagger} e^{-i\mathbf{k}\cdot\mathbf{r}_{i}},$$

$$a_{\mathbf{k}'}^{\dagger}(i) = a_{\mathbf{k}'}^{\dagger} e^{-i\mathbf{k}'\cdot\mathbf{r}_{i}}.$$
(4.B.2)

Note that all the termsin square brackets for the final equation vanish when averaged for stars, phase-diffused lasers, thermal light, and atoms. Therefore, keeping only the underlined terms, we find

$$G^{(2)}(\mathbf{r}_{1}, \mathbf{r}_{2}; t, t) = \mathscr{E}_{\mathbf{k}}^{4} \langle a_{\mathbf{k}}^{\dagger} a_{\mathbf{k}}^{\dagger} a_{\mathbf{k}} a_{\mathbf{k}} + a_{\mathbf{k}'}^{\dagger} a_{\mathbf{k}'}^{\dagger} a_{\mathbf{k}}' a_{\mathbf{k}}' + a_{\mathbf{k}}^{\dagger} a_{\mathbf{k}'}^{\dagger} a_{\mathbf{k}} a_{\mathbf{k}'} [1 + e^{-i(\mathbf{k} - \mathbf{k}') \cdot (\mathbf{r}_{1} - \mathbf{r}_{2})}] + a_{\mathbf{k}'}^{\dagger} a_{\mathbf{k}}^{\dagger} a_{\mathbf{k}'} a_{\mathbf{k}} [1 + e^{i(\mathbf{k} - \mathbf{k}') \cdot (\mathbf{r}_{1} - \mathbf{r}_{2})}] \rangle.$$

$$(4.B.3)$$

Problems

4.1 Show that the radiation field state which is a linear superposition of the vacuum state and a single photon state, i.e.,

$$|\psi\rangle=a_0|0\rangle+a_1|1\rangle,$$

where a_0 and a_1 are complex coefficients, is a nonclassical state.

4.2 Let $m_n = \langle a^{\dagger n} a^n \rangle$ be the *n*th-order moment of the intensity variable. Consider the matrix defined by

$$\mathcal{M} = \begin{bmatrix} 1 & m_1 & m_2 \\ m_1 & m_2 & m_3 \\ m_2 & m_3 & m_4 \end{bmatrix}.$$

Show that for a classical *P*-representation det *M* must be positive definite. (Hint: see G. S. Agarwal and K. Tara, *Phys. Rev. A* 46, 485 (1992).)

4.3 Consider a state described by the density operator

$$\rho = \mathcal{N}a^{\dagger m}e^{-\kappa a^{\dagger}a}a^{m},$$

where \mathcal{N} is a normalization constant and $\kappa = \hbar v/k_{\rm B}T$.

- (a) Show that it goes over to a Fock state if $\kappa \to \infty$ and to a thermal state if $\kappa \to 0$.
- (b) Find $g^{(2)}(0)$ and show that the photon statistics are sub-Poissonian if

$$\bar{n} < \sqrt{\frac{m}{m+1}},$$

where
$$\bar{n} = [\exp(\kappa) - 1]^{-1}$$
.

4.4 Find the photoelectron distribution function P_m for the coherent state $|\alpha\rangle$, the number state $|n\rangle$, and the single-mode thermal field at temperature T.

References and bibliography

Review articles on optical coherence theory

- R. J. Glauber, in *Quantum Optics and Electronics*, Les Houches, ed. C. DeWitt, A. Blandin, and C. Cohen-Tannoudji (Gordon and Breach, New York 1965).
- L. Mandel and E. Wolf, Rev. Mod. Phys. 37, 231 (1965).
- L. Mandel and E. Wolf, editors, Selected Papers on Coherence and Fluctuations of Light, Vols. 1 and 2 (Dover, New York 1970). These volumes contain an excellent collection of papers on optical coherence theory until 1966.
- R. J. Glauber, in *Quantum Optics*, ed. S. Kay and A. Maitland (Academic, New York 1970).
- L. Mandel, in *Progress in Optics*, Vol. 13, ed. E. Wolf (North-Holland, Amsterdam 1976).
- R. Loudon, Rep. Prog. Phys. 43, 913 (1980).
- H. Paul, Rev. Mod. Phys. 54, 1061 (1982).

Sagnac interferometry and ring laser gyroscope

- G. Sagnac, C. R. Acad. Sci. 157, 708 (1913).
- F. Aronowitz, in *Laser Applications*, ed. M. Ross (Academic, New York 1971), p. 113.
- W. W. Chow, J. Gea-Banacloche, L. M. Pedrotti, V. E. Sanders, W. Schleich, and M. O. Scully, *Rev. Mod. Phys.* 57, 61 (1985).

Applications of ring laser gyroscopes to general relativity

- M. O. Scully, M. S. Zubairy, and M. P. Haugan, Phys. Rev. A 24, 2009 (1981).
- W. Schleich and M. O. Scully, 'General Relativity and Modern Optics' in Modern Trends in Atomic and Molecular Physics, Proceedings of Les Houches Summer School, Session XXXVIII, ed. R. Stora and G. Grynberg (North-Holland, Amsterdam 1984).

Hanbury-Brown-Twiss experiment

- H. Hanbury-Brown and R. Q. Twiss, *Phil. Mag.* **45**, 663 (1954); *Nature* **178**, 1046 (1956); *Proc. Roy. Soc.* **A242**, 300 (1957).
- A. Forrester, R. Gudmundsen, and P. Johnson, Phys. Rev. 99, 1691 (1955).
- E. M. Purcell, *Nature* 178, 1449 (1956).
- U. Fano, Am J. Phys. 29, 539 (1961).
- G. Baym, Lectures on Quantum Mechanics, (Benjamin Pub., New York 1969), p. 431.
- R. Hanbury-Brown, *The Intensity Interferometer* (Taylor and Frances, London 1974).

Two-photon correlation experiment

- L. Mandel, Phys. Rev. A 28, 929 (1983).
- R. Ghosh and L. Mandel, Phys. Rev. Lett. 59, 1903 (1987).
- Z. Y. Ou and L. Mandel, Phys. Rev. Lett. 62, 2941 (1989).

Photon counting and photon statistics

- L. Mandel, Proc. Phys. Soc. 72, 1037 (1958).
- L. Mandel, in *Progress in Optics*, Vol. 2, ed. E. Wolf (North-Holland, Amsterdam 1963), p. 181.
- P. L. Kelley and W. H. Kleiner, Phys. Rev. 136, A316 (1964).
- M. O. Scully and W. E. Lamb, Jr., Phys. Rev. 179, 368 (1969).

Power spectrum

- J. H. Eberly and K. Wódkiewicz, J. Opt. Soc. Am. 67, 1252 (1977). This paper discusses the power spectrum for nonstationary fields.
- J. H. Eberly, C. V. Kunasz, and K. Wódkiewicz, J. Phys. B 13, 217 (1980).
- J. D. Cresser, *Phys. Rep.* **94**, 47 (1983). This paper gives an exhaustive review of the subject.

Balanced homodyne detection

- H. P. Yuen and V. W. S. Chan, Opt. Lett. 8, 177 (1983).
- N. G. Walker and J. E. Carrol, Opt. Quantum Electron. 18, 355 (1986).